European Journal of Medicinal Chemistry 294 (2025) 117745

Contents lists available at ScienceDirect

European Journal of Medicinal Chemistry

journal homepage: www.elsevier.com/locate/ejmech

Discovery of LC-SF-14, a selective dual inhibitor of SHP2 and FGFR for the treatment of FGFR2-driven gastric cancer

Lei Zheng [a,1], Yuhan Wang [a,1], Zheng Jiang [a,1], Shiyan Chen [a], Xiansheng Cao [a], Xiaohao Huang [a], Ruixiang Luo [a], Lulu Zheng [b], Qin Li [a], Linglan Tu [a], Jie Li [c], Guang Liang [a,*], Lingfeng Chen [a,**]

[a] School of Pharmacy, Hangzhou Medical College, Hangzhou, 310014, Zhejiang, China
[b] Department of Pharmacy, Tongde Hospital of Zhejiang Province, Hangzhou, Zhejiang, 310000, China
[c] School of Medicine, Zhejiang University City College, Huzhou Road, Hangzhou, 310015, China

ARTICLE INFO

Keywords:
Receptor tyrosine kinase
Fibroblast growth factor receptor
Src homology-2 domain-containing phosphatase 2
Bifunctional molecule

ABSTRACT

Src homology-2 domain-containing phosphatase 2 (SHP2) and fibroblast growth factor receptor 2 (FGFR2) are oncoproteins. Despite the tremendous progress achieved with SHP2 allosteric inhibitors, the efficacy of single-agent SHP2 inhibitor treatments has been shown to be suboptimal, based on recent clinical trial results. A previous study demonstrated the synergistic effect of the allosteric SHP2 inhibitor SHP099 and the FGFR inhibitor BGJ398, suggesting a potential combined targeted therapeutic option for cancer. In this study, we discovered a potent SHP2 and FGFR2 dual inhibitor, LC-SF-14, using a linked pharmacophore strategy and structural optimization. The active compound LC-SF-14 exhibited high inhibitory potency against both targets (71.6 nM and 8.9 nM, respectively) with a high degree of selectivity, as verified by kinase kinome and protein tyrosine phosphatase (PTP) enzyme profiling. LC-SF-14 effectively prevented the phosphorylation of FGFR2 and downstream signaling, resulting in tumor regression *in vivo*. These results indicate that the bifunctional molecule LC-SF-14, the first PTP- and receptor tyrosine kinase (RTK)-targeted dual inhibitor, is a promising lead for the treatment of cancers bearing SHP2 and FGFR oncogenic drivers.

1. Introduction

Levels of protein tyrosine phosphorylation are maintained by the opposing actions of receptor tyrosine kinases (RTKs) and protein tyrosine phosphatases (PTPs), which modify the addition or removal of phosphate groups to or from proteins. The *PTPN11* gene encodes the protein Src homology-2 domain phosphatase 2 (SHP2), which participates in a variety of signaling pathways, including the RAS-RAF-ERK pathway [1]. Almost all RTKs trigger the RAS signaling pathway through the activation of SHP2 [2]. This key protein is a unique proto-oncogene within the PTP family, and abnormal SHP2 activation has been linked to certain cancers [3–6]. Thus, SHP2 is an optimal target for cancer therapeutics [7].

SHP2 is comprised of two Src homology-2 (SH2) domains and a PTP domain. Under resting conditions, SHP2 remains in an autoinhibited state where the N-SH2 domain blocks the catalytic site of the PTP domain, thereby blocking the substrate from binding and suppressing SHP2 activity [8]. However, the development of selective SHP2 orthostatic inhibitors is challenging due to the highly conserved catalytic site among the PTP family [9–13]. The year 2016 was a turning point in SHP2-based drug discovery when the first "tunnel" allosteric site SHP2 inhibitor SHP099 was discovered [14]. Since then, a series of SHP2 allosteric inhibitors, namely TNO155 [12], RMC-4630 [15], and JAB-3312 [16,17], have entered clinical trials for the treatment of cancer.

Despite the tremendous progress achieved in SHP2 allosteric inhibitors, single-agent SHP2 inhibitor treatments have shown limited benefit in patients [18]. In 2021, Novartis revealed data from a

This article is part of a special issue entitled: Enzyme inhibitors published in European Journal of Medicinal Chemistry.

* Corresponding author. Hangzhou Medical College, Hangzhou, 310012, China.
** Corresponding author. Hangzhou Medical College, Hangzhou, 310012, China.
E-mail addresses: wzmcliangguang@163.com (G. Liang), lfchen@hmc.edu.cn (L. Chen).

[1] These authors contributed equally to this work.

https://doi.org/10.1016/j.ejmech.2025.117745
Received 2 April 2025; Received in revised form 1 May 2025; Accepted 7 May 2025
Available online 11 May 2025

dose-finding study of TNO155 in adult patients with advanced solid tumors (NCT03114319). The trial included 118 patients, with only 20 % reaching stable disease (SD) and a median SD duration of 4.9 months. In the same year, Novartis terminated the single-agent clinical trial of TNO155 [19]. Although clinical trials of SHP2 inhibitor monotherapies have been suspended, SHP2 inhibitor-based combination therapies have shown promising results. Studies on SHP2 inhibitors in combination with other inhibitors, including EGFR inhibitors, KRAS G12C inhibitors, CDK4/6 inhibitors, anti-PD-1 antibodies, and BRAF inhibitors, are ongoing (NCT03114319, NCT04330664, NCT04000529, NCT04294160) [20–22]. Notably, the SHP2 inhibitor JAB-3312 combined with the KRAS G12C inhibitor was the first to enter phase 3 clinical trials for the treatment of advanced non-small cell lung cancer with KRAS mutation (NCT06416410) [16].

The fibroblast growth factor receptor (FGFR1-4) family is an important RTK subfamily involved in regulating numerous physiological processes [23,24]. Upon ligand binding, two direct substrates of FGFR, FRS2α, and PLCγ, activate multiple cascade pathways, including the SHP2-MAPK-, PI3K-, and STAT-dependent signaling pathways. Dysregulation of FGFR signaling caused by amplification, point mutations, or gene fusions results in oncogenesis and tumor progression [24–27]. FGFR1-4 amplification is frequently detected in patients with advanced solid tumors [28]. Specifically, the overall survival of gastric cancer patients is closely associated with the overexpression of FGFR2 [29–31]. Selective FGFR inhibitors, such as infigratinib (BGJ398), pemigatinib, and erdafitinib, have been developed [32–36]. Pemigatinib has been approved by the US Food and Drug Administration (FDA) for the treatment of patients with FGFR2 rearrangements [37].

Recent studies have shown that combination therapy targeting SHP2 and FGFR has a synergistic effect in FGFR-driven cancer [38,39]. In these studies, the inhibition of SHP2 with SHP099 led to the suppression of leukemogenesis in models of stem cell leukemia/lymphoma syndrome (SCLL), and the combined targeting of SHP2 and FGFR indicates a better treatment regimen. Despite promising preclinical results, concerns remain regarding combination chemotherapy involving the two inhibitor systems. Currently, developing a single molecule able to specifically and simultaneously interact with multiple targets is gaining key consideration in contemporary drug discovery paradigms [40]. In recent years, dual-target inhibitors have emerged, which are able to improve the antitumor effect and avoid resistance by synergistically targeting the

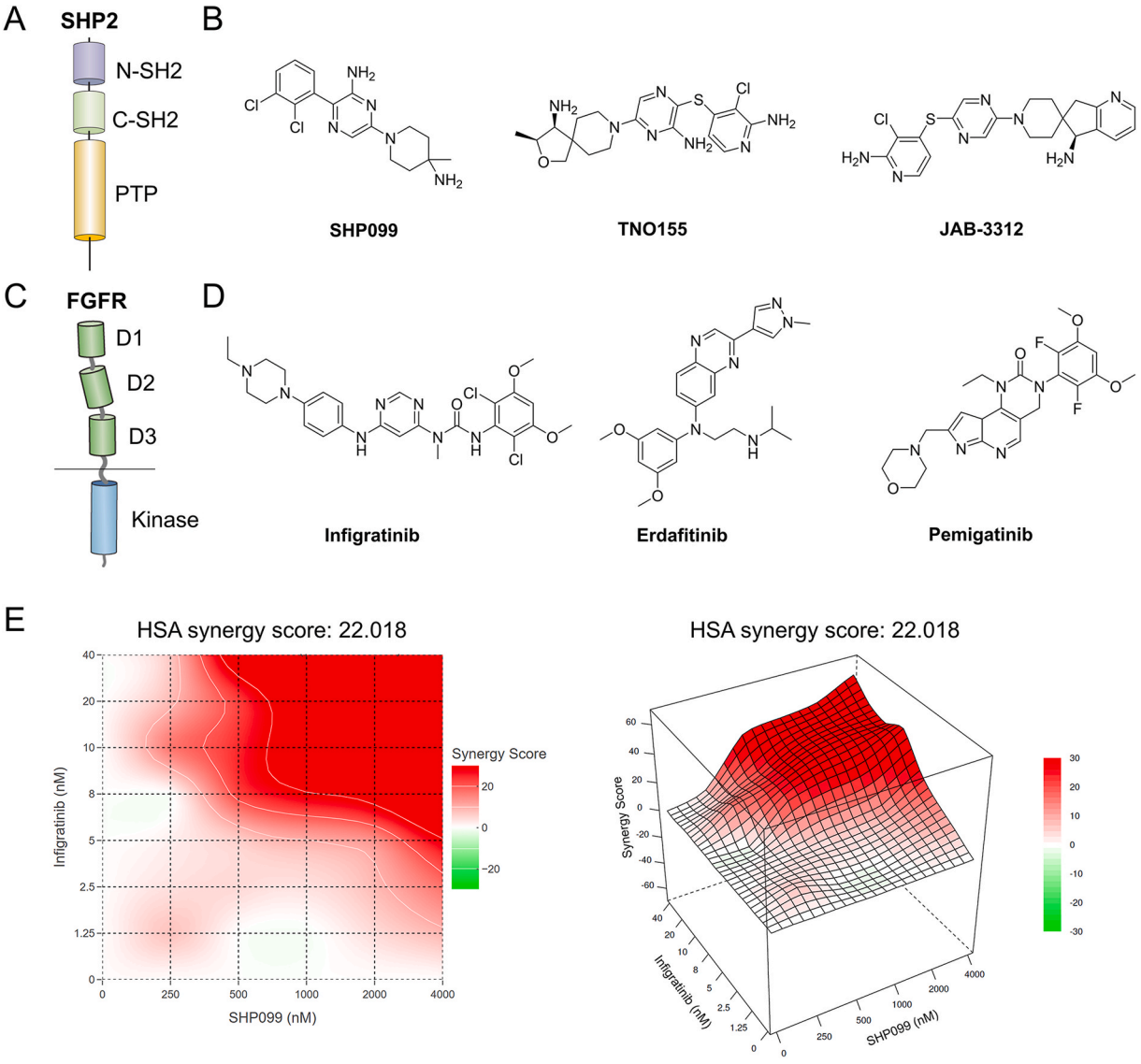

Fig. 1. SHP2 and FGFR inhibitors. (A) Schematic illustration of SHP2 domains containing N-SH2, C-SH2, and protein tyrosine phosphatase (PTP) domains. (B) Reported SHP2 allosteric inhibitors. (C) A schematic graph showing the architecture of FGFR domains. (D) Reported FGFR inhibitors. (E) Synergistic effect of FGFR inhibitor infigratinib and SHP2 inhibitor SHP099 in KATOIII cells. The figures were generated using SynergyFinder (https://synergyfinder.org).

two targets. Designing multi-target drugs has obvious clinical advantages compared with combination drug therapy. With the reduction of treatment complexity, it can reduce drug side effects, pharmacokinetic complexity, and drug-drug interactions, and improve patient compliance [41]. In addition, the regulation of multiple biological targets may enhance the therapeutic effect through synergistic effects [40,42]. A few SHP2-related bifunctional molecules are designed with improved anti-cancer activity, including SHP2/HDAC and SHP2/CDK4 dual inhibitors [19,43,44].

Herein, we provide the first evidence of the feasibility of rationally designing a dual inhibitor against both PTP and RTK that is highly selective for its intended targets, SHP2 and FGFR. A structure-based drug design strategy was used to identify potent SHP2/FGFR dual inhibitors. Pivotal structure-activity relationship (SAR) studies have led to the development of LC-SF-14, a promising lead for cancer treatment.

2. Results

2.1. Rational design strategy for SHP2 and FGFR dual inhibitors

Firstly, we investigated the synergistic effect of the dual inhibition of FGFR and SHP2 via synergy matrix analysis. KATOIII cell lines were cotreated with gradients concentrations of FGFR inhibitor infigratinib and SHP2 inhibitor SHP099. HSA synergy score >0 designates a synergistic effect. As shown in Fig. 1E, cotreatment with infigratinib and SHP099 showed pronounced synergistic effects in inhibiting KATOIII cell proliferation (HSA synergy score = 22.018). This result indicated co-targeting SHP2 and FGFR may offer a promising therapeutic option.

Next, a structure-based drug design strategy was used to develop dual inhibitors capable of targeting both SHP2 and FGFR by analyzing the known structural features of SHP099 and BGJ398 (infigratinib) bound to SHP2 and FGFR1, respectively. Based on the co-crystal structure of the SHP2-SHP099 (PDB: 5EHR) complex, both the left-side piperidinamine motif and the right-side 2,3-dichlorophenyl motif in SHP099 point towards the solvent (Fig. 2A). We preferentially focused on the right dichlorophenyl region as the potential tethering site for bifunctional molecule design as the amino aromatic region is well tolerated with various substituents and the polar interactions of the piperidinamine motif with SHP2 are essential [44,45]. On the other hand, we leveraged the binding mode of BGJ398 in the FGFR kinase domain, which indicated that the piperazine group was exposed to the solvent region; therefore, it could be utilized as a suitable linker tethering site bifunctional molecule such as proteolysis-targeting chimeric (PROTAC) as described in our recent study (Fig. 2B) [46]. Accordingly, we designed and synthesized dual inhibitors of SHP2 and FGFR for the first time via a fused pharmacophore strategy and evaluated these compounds *in vitro* and *in vivo*.

2.2. Enzyme inhibitory activity screening and SAR study

To test our hypothesis, compound **1** was synthesized by merging the FGFR inhibitor BGJ398 and SHP2 inhibitor SHP099 to assess its enzymatic activities. 3-amino-2-chlorobenzenethiol hydrochloride and 3-bromo-6-chloropyrazin-2-amine were subjected to a Cu(I)-catalyzed cross-coupling reaction to produce the SHP2-binding part (Scheme 1). The FGFR binding motif was obtained through an S_NAr reaction with 4,6-dichloropyropyridine and *tert*-butyl 4-(4-aminophenyl)piperazine-1-carboxylate (Scheme 2). Finally, the synthesis of compound **1** was achieved by connecting the SHP2-binding part with the FGFR-binding part using methyl 3-chloro-3-oxopropanoate as a linker (Scheme 2).

To guide the SAR studies, *in vitro* enzymatic assays for SHP2 and FGFR were developed [14,46]. As shown in Table 1, although low SHP2 inhibitory activity was observed, with a half-maximal inhibitory concentration (IC_{50}) of 1549 nM, compound **1** exhibited high inhibition potency against the purified FGFR2 kinase domain, with an IC_{50} value of 42.2 nM, thus providing a good lead for further optimization.

Previous studies have shown that the length and properties of the linker affect the activity of bifunctional molecules. We envisioned that linker length optimization could improve SHP2 inhibitory activity. Thus, compounds **2** (LC-SF-14) and **3** with different alkyl linkers were designed and synthesized to improve dual-target inhibition capability, especially for SHP2. To our delight, compound **2** exhibited improved inhibition potency against SHP2 and FGFR2 with IC_{50} values of 71.6 and 8.9 nM, respectively. LC-SF-14 was ~21-fold and 5-fold more potent than lead compound **1** against SHP2 and FGFR2, respectively. Surprisingly, further attempts to increase the alkyl linker length (compound **3**) lowered the SHP2 binding affinity, with an IC_{50} value of 614 nM. These results demonstrate that linker length can have a considerable influence on the efficacy of bifunctional molecules. The various linkers of LC-SF-14 may lead to different conformations of the binary complexes, thus serving as key factors contributing to SHP2 and FGFR inhibition.

We further modified the structure of compound **2** in order to explore

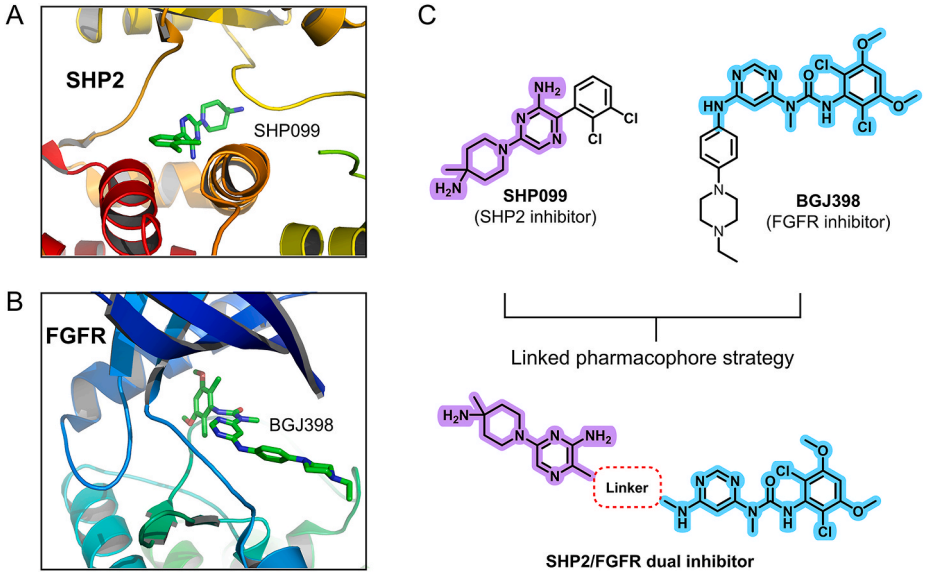

Fig. 2. Rationale of the SHP2 and FGFR dual inhibitors. (A) Structure of the SHP099-SHP2 and BGJ398 (infigratinib)-FGFR1 co-crystal complexes. (B) Design strategy for SHP2 and FGFR dual inhibitors.

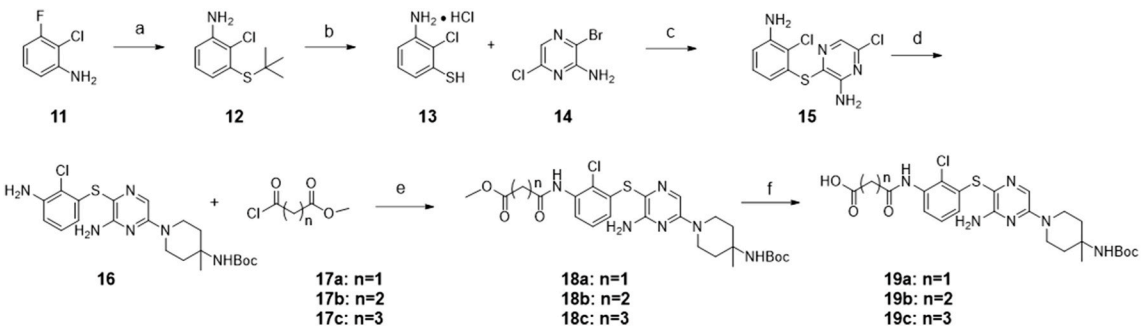

Scheme 1. Synthesis of Target Compounds **19a**-**19c**:Reagents and conditions: (a) *tert*-butylthiol, Cs_2CO_3, DMF, 120 °C, 36 h; (b) conc. HCl, 80 °C, 6 h; (c) K_3PO_4, CuI, 1,4-dioxane, 1,10-phenanthroline, 90 °C, 20 h; (d) DIPEA, DMSO, 100 °C, 6 h; (e) DIPEA, DCM, 0 °C-rt, 1 h; (f) LiOH–H_2O, THF, Methanol, H_2O, 0 °C-rt, 3 h.

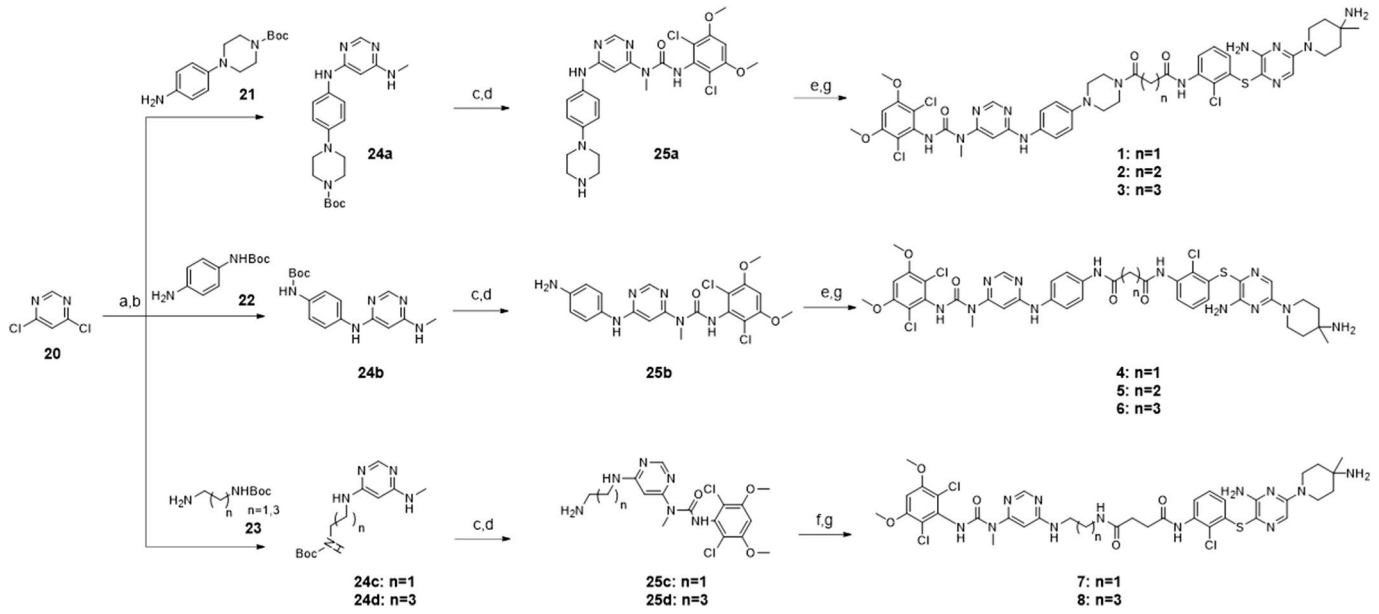

Scheme 2. Synthesis of Target Compounds **1**–**8**: Reagents and conditions: (a) DIPEA, IPA, DMF, 40 °C, 18 h; (b) methylamine, 1-Butanol, DIPEA, 120 °C, 12 h; (c) DIPEA, toluene, 80 °C, 16 h; (d) TFA, DCM, rt, 2 h, (e) **19a-c**, HATU, DIPEA, DMF, rt, 2 h; (f) **19b**, HATU, DIPEA, DMF, rt, 2 h; (g) TFA, DCM, rt, 2 h.

the SAR. we designed compounds **4**–**6**, which differ from compounds **1**–**3** by the absence of a piperazine group, in order to explore the effect of the piperazine group in the linker chain on activity (Scheme 2). The results indicated that the binding affinity of compounds **4**–**6** to SHP2 tunnel site is considerably diminished following the elimination of the piperazine ring, although compound **4** continues to exhibit a degree of inhibitory effect on FGFR2. Furthermore, to further explore the linker, we replaced the aryl piperazine group in compound **1** with different alkyl linkers yielding compounds **7** and **8**. It was observed that the two compounds exhibited a complete loss of inhibitory efficacy against both SHP2 and FGFR upon the removal of the piperazine moiety and the benzene ring (Table 1). This suggests that these structural moieties are crucial for the compounds' bioactivity against both targets.

Finally, we studied the effect of a longer flexible linker on activity and synthesized compounds **9** and **10** (Scheme 3). However, these two compounds did not exhibit improved FGFR and SHP2 inhibitory activities *in vivo*. Together, these results suggest that the aryl piperazine fragments may play a critical role in maintaining the activity of the FGFR/SHP2 dual inhibitors. The promising enzymatic data for the active compound LC-SF-14 validated that our design strategy for SHP2/FGFR bifunctional molecules was feasible, and LC-SF-14 was subjected to further investigations.

2.3. LC-SF-14 is a potent dual inhibitor of SHP2 and FGFR2

Owing to its bifunctional properties, LC-SF-14 is considered able to simultaneously interact with FGFR kinase and its downstream adaptor protein SHP2 among RTK signaling, thereby blocking SHP2 docking to the long tail of FRS2α (Fig. 3A–B). Compound LC-SF-14 showed a low IC_{50} value against full-length SHP2 The dose-response 6,8-difluoro-4-methylumbelliferyl phosphate (DiFMUP) biochemical assay for LC-SF-14 is shown in Fig. 3C. To verify the allosteric binding site of LC-SF-14, compound LC-SF-14 was chosen for further *in vitro* studies. A truncated SHP2 protein ($SHP2^{PTP}$) and a tunnel site binding-deficient mutant ($SHP2^{T253M/Q257L}$) were constructed and purified for the DiFMUP biochemical assay as previous described [47]. The $SHP2^{PTP}$ mutant caused SH2 domain reorganization and a missing tunnel site, while the $SHP2^{T253M/Q257L}$ mutant was designed to disrupt the interaction between LC-SF-14 and the SHP2 tunnel site. As shown in Fig. 3D–F, both mutations completely abolished the SHP2 inhibitory activity of LC-SF-14, suggesting that LC-SF-14 inhibits the catalytic activity of SHP2 via direct binding to its tunnel allosteric site and stabilizes the enzyme in the inactive conformation.

Infigratinib, the parental FGFR binding component of LC-SF-14, is a pan-FGFR inhibitor. Thus, we next investigated the target selectivity of LC-SF-14 among the four conserved FGFR subfamily member including FGFR1-4. Compared to FGFR2, LC-SF-14 showed moderate selectivity

Table 1
In vitro SHP2 and FGFR inhibitory activities of target compounds

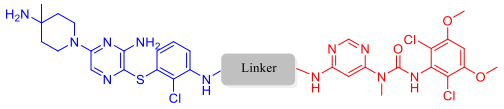

Compds	Linker	Kinase inhibition (IC_{50} nM)	
		SHP2	FGFR2
1	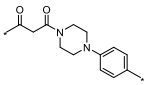	1549	42.2
2 (LC-SF-14)	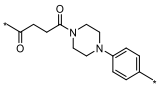	71.6	8.9
3	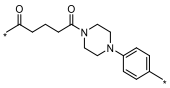	614.0	124.4
4	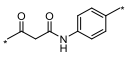	246.1	49.3
5	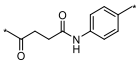	310.8	131.2
6	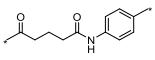	145.8	110.2
7	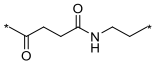	1008	300.8
8	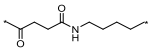	749.3	827.6
9	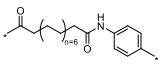	4199	473.2
10	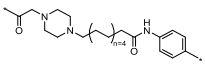	2690	313.5
SHP099	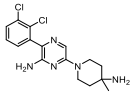	72.37	>10000
Infigratinib	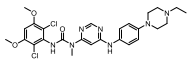	>10000	4.5

for FGFR1 (~3.6-fold) and FGFR3 (~5.1-fold) in biochemical assays (Fig. 3G–I). Remarkably, LC-SF-14 demonstrated >1000-fold selectivity for FGFR4 (Fig. 3J). The kinase domain of FGFR4 is structurally divergent from that of FGFR1-3. Previous studies have indicated that FGFR4 inhibition is related to adverse effects in the clinic; thus, these data indicated the increased overall safety profile of LC-SF-14 [48]. The high potency of LC-SF-14 against FGFR2 revealed a biochemical profile distinctly different from that of the lead compound infigratinib. The unique FGFR2 selectivity of LC-SF-14 may originate from the fact that after the SHP099 fragment is linked, it affects the interaction between infigratinib and other isoforms (FGFR1/3/4).

To investigate whether compound LC-SF-14 exhibits dual-binding capability to FGFR kinase and its downstream adaptor protein SHP2, we employed a biolayer interferometry (BLI)-based ternary complex formation assay. In this established protocol, biotinylated FGFR2 kinase domain ($FGFR2^{KD}$) was immobilized onto streptavidin-coated sensor tips. The functionalized sensors were first incubated with LC-SF-14-containing buffer to allow compound binding, followed by exposure to full-length SHP2 solution to assess ternary complex formation. As illustrated in Fig. 3K, LC-SF-14 demonstrated direct binding to $FGFR2^{KD}$, forming a binary $FGFR2^{KD}$-LC-SF-14 complex. Remarkably, this binary complex exhibited specific binding affinity for SHP2, resulting in the formation of a tertiary FGFR2-LC-SF-14-SHP2 complex. Control experiments conducted in the absence of LC-SF-14 revealed no detectable direct interaction between FGFR2 and SHP2 (Fig. 3L). These findings strongly suggest that LC-SF-14 possesses the molecular capacity to simultaneously engage both FGFR kinase and its downstream effector SHP2, potentially enabling dual-target modulation in cellular systems. Based on these promising biochemical results, LC-SF-14 was selected for the treatment of FGFR2-driven cancer *in vivo*.

2.4. *LC-SF-14 inhibits FGFR2-FRS2α-SHP2-MAPK signaling and suppresses the proliferation of gastric cancer cells*

Next, we assessed the functional consequences of LC-SF-14-mediated dual SHP2 and FGFR inhibition in FGFR2-driven cancer cells. As the proliferation of KATOIII cells were strongly driven by FGFR2-FRS2α-SHP2 signaling, we examined the anti-proliferative effects of LC-SF-14. The anti-proliferative IC_{50} of LC-SF-14 was 9.2 nM after 72 h of incubation (Fig. 4A). In contrast, SHP099 and infigratinib exhibited 179- and 2-fold lower potencies, respectively, as demonstrated by the KATO III proliferation assay, with IC_{50} values of 1650 and 18.6 nM, respectively.

We next evaluated the effect of LC-SF-14 on FGFR-SHP2 signalling in KATOIII and SNU16 cells. Levels of pFGFR, pERK, and pP90RSK in cells were evaluated after 12 h of incubation with infigratinib, SHP099 or LC-SF-14 at 20 nM. As shown in Fig. 4B–C, FGFR phosphorylation was significantly suppressed upon infigratinib and LC-SF-14 treatment. These results indicated that LC-SF-14 retained its inhibition potency against FGFR. Further, we verified the inhibitory activities of different compounds on the phosphorylation level of SHP2 downstream protein pERK and pP90RSK (Fig. 4B–C). The results showed that LC-SF-14 exhibited stronger downstream protein phosphorylation inhibition than infigratinib and SHP099. These results suggest that dual inhibition of FGFR and SHP2 can more effectively inhibit the FGFR2 downstream signalling. In addition, the immunofluorescence results showed that LC-SF-14 exhibited a stronger inhibitory effect against ERK phosphorylation than the two parental compounds (Fig. 4D). We also examined the gene expression of dual specificity phosphatase 6 (*DUSP6*), a phosphatase and negative regulator of ERK [20]. Compared to treatment with infigratinib or SHP099 alone, dual inhibitor LC-SF-14 treatment led to greater suppression of *DUSP6* expression (Fig. 4E). The toxicity of LC-SF-14 to HEK293T cells was further evaluated. The result indicated that LC-SF-14 showed no significant inhibitory activity HEK293T with low FGFR2 expression (Fig. S1). Taken together, this cellular evidence indicates the advantages of co-targeting SHP2 and FGFR2.

2.5. *Binding mode of the SHP2-FGFR2 dual inhibitor*

To explore the target binding mode of the newly discovered SHP2/FGFR2 dual inhibitor, LC-SF-14 was docked to the tunnel allosteric binding site of SHP2 and the kinase domain of FGFR2. As shown in Fig. 5A, the SHP2 binding part of the bifunctional molecule LC-SF-14 was bound to the tunnel site created through the interface of the PTP and two SH2 domains. LC-SF-14 forms key hydrogen bonds with Glu-249 and Glu-250 from the PTP domain of SHP2 and Phe-113 from the N-SH2 and C-SH2 linkers. Compared with the parent compound SHP099, the introduction of a carbonyl group in the linker of LC-SF-14 formed extra hydrogen bonds with Arg-111 from the linker of the two SH2 domains. The FGFR binding region of LC-SF-14 occupies the kinase domain in a manner similar to that of infigratinib. In particular, LC-SF-14 formed two key hydrogen bonds in the backbone hinge region of

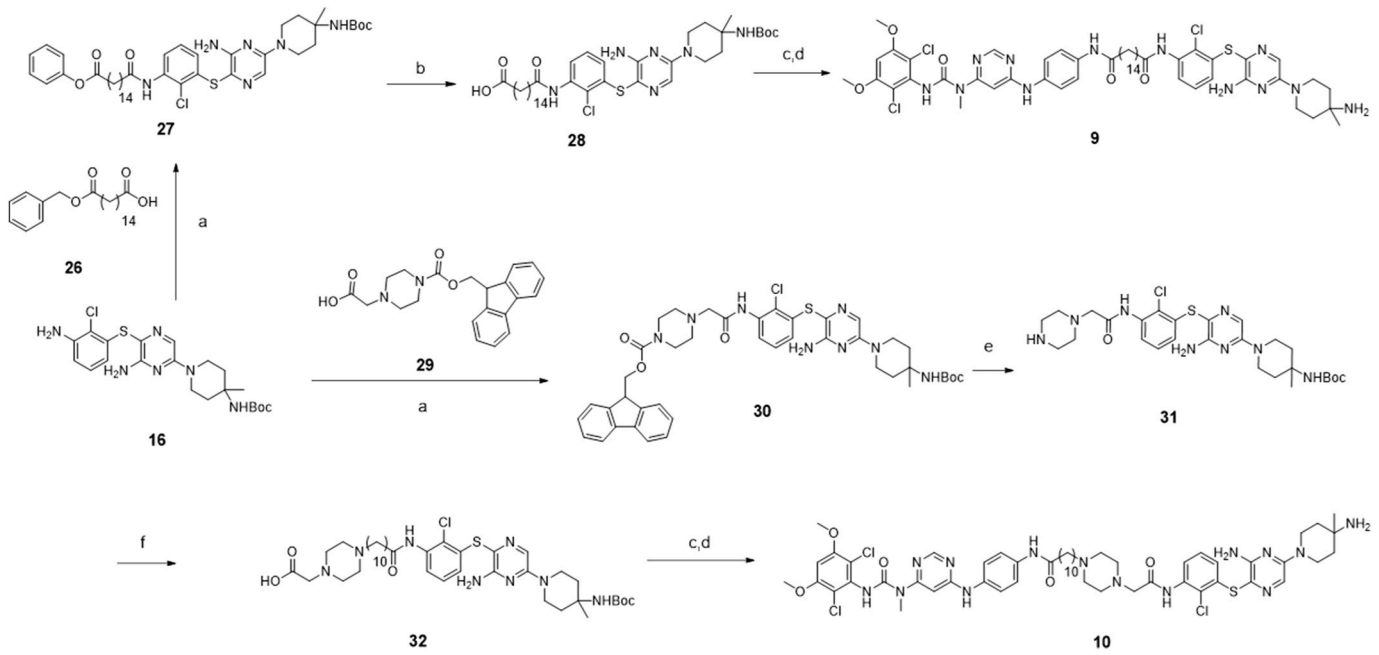

Scheme 3. Synthesis of Target Compounds **9 and 10**: Reagents and conditions: (a) TCFH, NMI, THF, MeCN, 6 h, rt; (b) NaOH, MeOH, THF, H_2O, rt, 8 h; (c) **25b**, HATU, DIPEA, DMF, rt, 2 h; (d) TFA, DCM, rt, 2 h; (e) piperidine, MeCN, rt, 2 h; (f) 11-bromoundecanoic acid, K_2CO_3, KI, DMF, 60 °C, 12 h.

FGFR2 (Fig. 5B). The substitution at the 4-position fits into the hydrophobic pocket of the kinase, whereas the linker and SHP2 binding part faces outward to the solvent area of FGFR. Collectively, the putative docking results revealed a favorable binding mode for the SHP2/FGFR2 dual inhibitor LC-SF-14 and demonstrated its potent inhibitory activity against both SHP2 and FGFR2.

2.6. Selectivity study of LC-SF-14 against PTPs and kinases

Because of the highly conserved RTK and PTP catalytic domains, it is challenging to discover selective inhibitors [49]. To investigate the selective profile of compound LC-SF-14, inhibitory activities were screened among a panel of kinases and mammalian PTPs. LC-SF-14 was tested against a panel of 80 kinases at 1 μM (Fig. 5C and Table S1). This kinome screening result showed compound LC-SF-14 had a potent inhibitory effect on FGFR2 (inhibition rate = 99.7 %) and had no obvious off-targets among all the other tested kinases (inhibition rate <30 %).

On the other hand, to investigate the selectivity of compound LC-SF-14 among PTPs, a panel of 7 representative different types of PTP enzymes were expressed and purified, including a receptor type PTP (PTPRA), two non-receptor PTPs (PTPN1 and PTPN12), a VH1-like PTP (PRL2), and a class II PTP (LMW-PTP). As shown in Fig. 5D, LC-SF-14 showed no significant inhibitory activity against other PTPs. A high level of target selectivity of LC-SF-14 was achieved owing to the unique allosteric site of SHP2 among all PTP families.

2.7. Evaluation of LC-SF-14 in vivo

Based on the high selectivity and potency of LC-SF-14, we next assessed the efficacy of LC-SF-14 *in vivo*. We evaluated the pharmacokinetic properties (PK) of LC-SF-14 in rats (Table S2). The results indicated that the bifunctional molecule LC-SF-14 displayed unfavorable PK properties with low oral bioavailability (F = 2.6 %), which may be due to its relatively high molecular weight and lipophilicity. Thus, the *in vivo* antitumor efficacy of LC-SF-14 was evaluated by intraperitoneal injection (i.p.).

The FGFR2-overexpressed gastric cancer cell line SNU-16 (FGFR2-amplified) was used to assess the *in vivo* activity of LC-SF-14. Nude mice with subcutaneous SNU-16 xenografts were intraperitoneally injected with LC-SF-14 at doses of 10 and 20 mg/kg daily. The administration of LC-SF-14 achieved 41.06 % and 85.62 % growth inhibition, respectively (Fig. 6A–C). No body weight loss was observed in mice receiving low or high doses of LC-SF-14 (Fig. 6D).

To further investigate the efficacy of the dual inhibitor LC-SF-14 on FGFR2-SHP2-MAPK signaling *in vivo*, tumor tissues were analyzed by western blotting. LC-SF-14 administration resulted in significant inhibition against FGFR2 A-loop tyrosine as well as downstream PLCγ and Erk phosphorylation after 10 mg/kg dose daily treatment compared to the vehicle group (Fig. 6E). Notably, mice which received a 20 mg/kg dose of LC-SF-14 had markedly decreased phosphorylation levels of FGFR2, PLCγ, and ERK1/2 in tumor tissue, which was also indicated by the Ki-67 staining results (Fig. 6F). Thus, LC-SF-14 is an efficient SHP2/FGFR2 dual inhibitor *in vivo* and a novel agent for FGFR2-driven gastric cancer treatment.

3. Discussion

The modulation of SHP2 activity is a promising strategy for treating RTK-related cancers. Since 2016, several SHP2 potent allosteric inhibitors have been developed for the treatment of solid tumors. Despite favorable preclinical results, the clinical performance of SHP2 inhibitors as monotherapy paradigms remains suboptimal [19]. Recently, SHP2 inhibitor-based combination therapies have emerged. The synergistic combination of SHP2 inhibitors with kinase inhibitors or antibodies shows significant benefits in enhancing therapeutic efficacy and overcoming resistance. An increasing number of clinical trials are investigating the outcomes of allosteric SHP2 inhibitors combined with inhibitors of EGFR, KRAS, CDK, MEK, and BRAF.

Compared with combination therapy using multiple drugs, dual-target inhibitors have shown advantages such as lower tissue toxicity and lower dosage requirements [50]. Based on the synergistic effect of the SHP2 inhibitor, SHP099, in combination therapy, significant evidence indicates the development of bifunctional molecules co-targeting SHP2 and FGFR may offer a promising therapeutic option for the treatment of FGFR-driven cancer.

In this study, we designed and synthesized a series of dual inhibitors of SHP2 and FGFR2 using a pharmacophore fusion strategy. Through

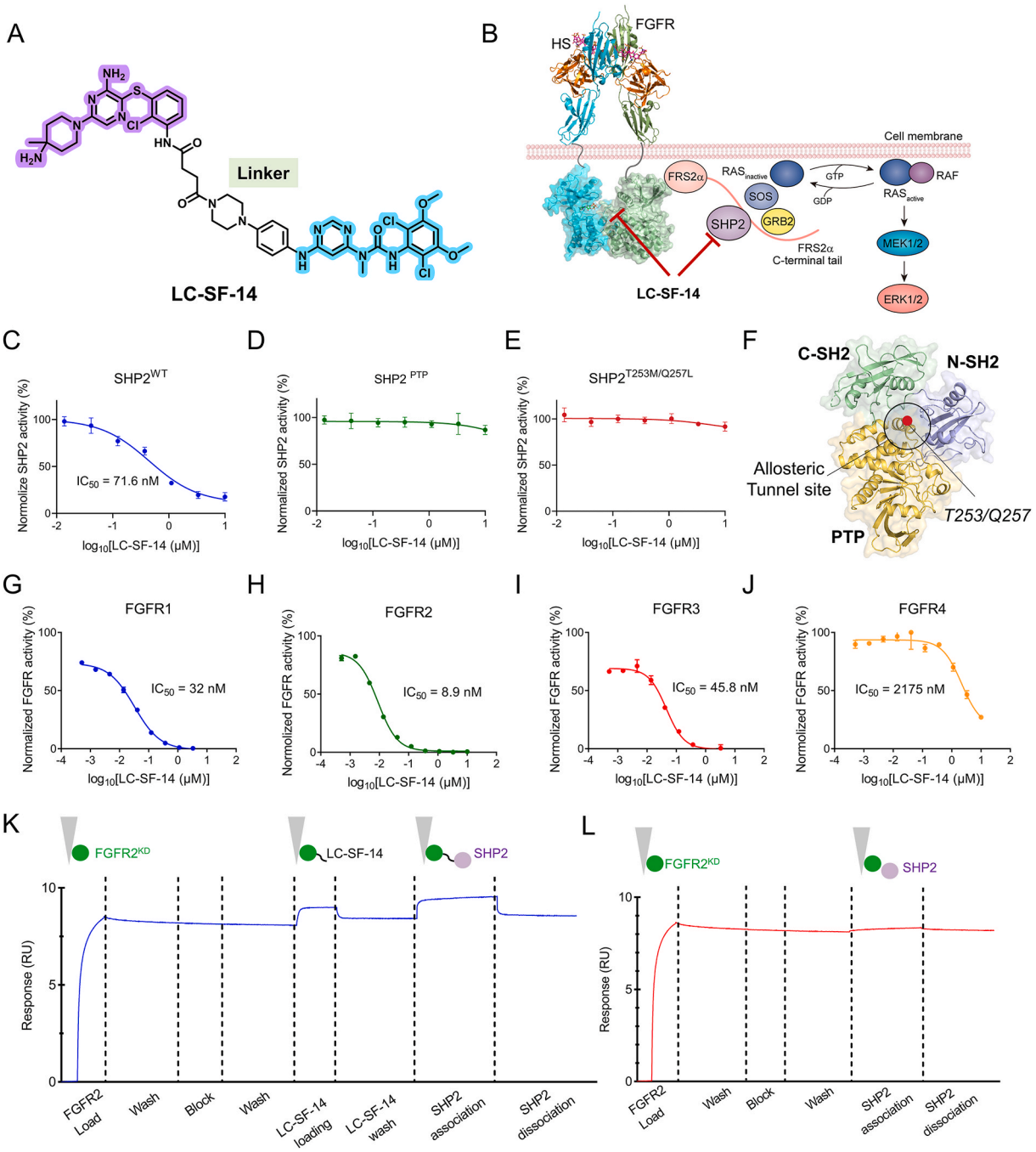

Fig. 3. Discovery of LC-SF-14 as a potent dual inhibitor of SHP2 and FGFR2. (A) Chemical structure of bifunctional LC-SF-14. (B) Schematic graph showing that LC-SF-14 simultaneously interacts with the FGFR kinase domain and the allosteric site of the downstream protein, SHP2. (C–E) Dose-response DiFMUP assays for LC-SF-14 with $SHP2^{WT}$ (C), $SHP2^{PTP}$ (D), and $SHP2^{T253M/Q257L}$ (E). (F) Sites with the T253 M/Q257L double mutation in the SHP2 tunnel site. N-SH2, C-SH2, and PTP domains are indicated in blue, green, and yellow, respectively. (G–J) Biochemical kinase inhibitory activity of LC-SF-14 against FGFR1−4. (K–L) Ternary complex (K) and binary complex (L) BLI assay illustrating immobilized $FGFR2^{KD}$ throughout noted the binding and wash steps ($FGFR2^{KD}$: 1.10 μg ml^{-1}, SHP2: 1.10 μg ml^{-1}).

structural optimization and SAR studies, we obtained compound LC-SF-14, a dual inhibitor of SHP2/FGFR2, which showed the most effective and balanced inhibitory activity. Our study demonstrates that linker length and composition work together to determine the potency of SHP2/FGFR2 dual inhibitors. Subsequent studies have shown that the rationally designed SHP2/FGFR2 dual inhibitor, LC-SF-14, shows high selectivity for RTKs and PTPs. The mechanism study further shows that the compound LC-SF-14 inhibits the growth of FGFR2-driven tumors by co-inhibiting FGFR2 and SHP2 and downregulating the expression of p-ERK and p-P90RSK. It also showed superior anti-proliferative activity against FGFR2-driven gastric cancer cell lines compared to the two parental inhibitors. To the best of our knowledge, this is the first report of a bifunctional molecule that co-targets RTK and PTP. However, LC-SF-14 exhibited relatively poor oral bioavailability in the plasma PK parameters of mice. Therefore, studies on the structural optimization of these derivatives are currently underway to achieve better plasma pharmacokinetic properties. In addition, the superior antiproliferative activity of LC-SF-14 has prompted us to further explore the efficacy of LC-SF-14 against other FGFR2-driven cancer types.

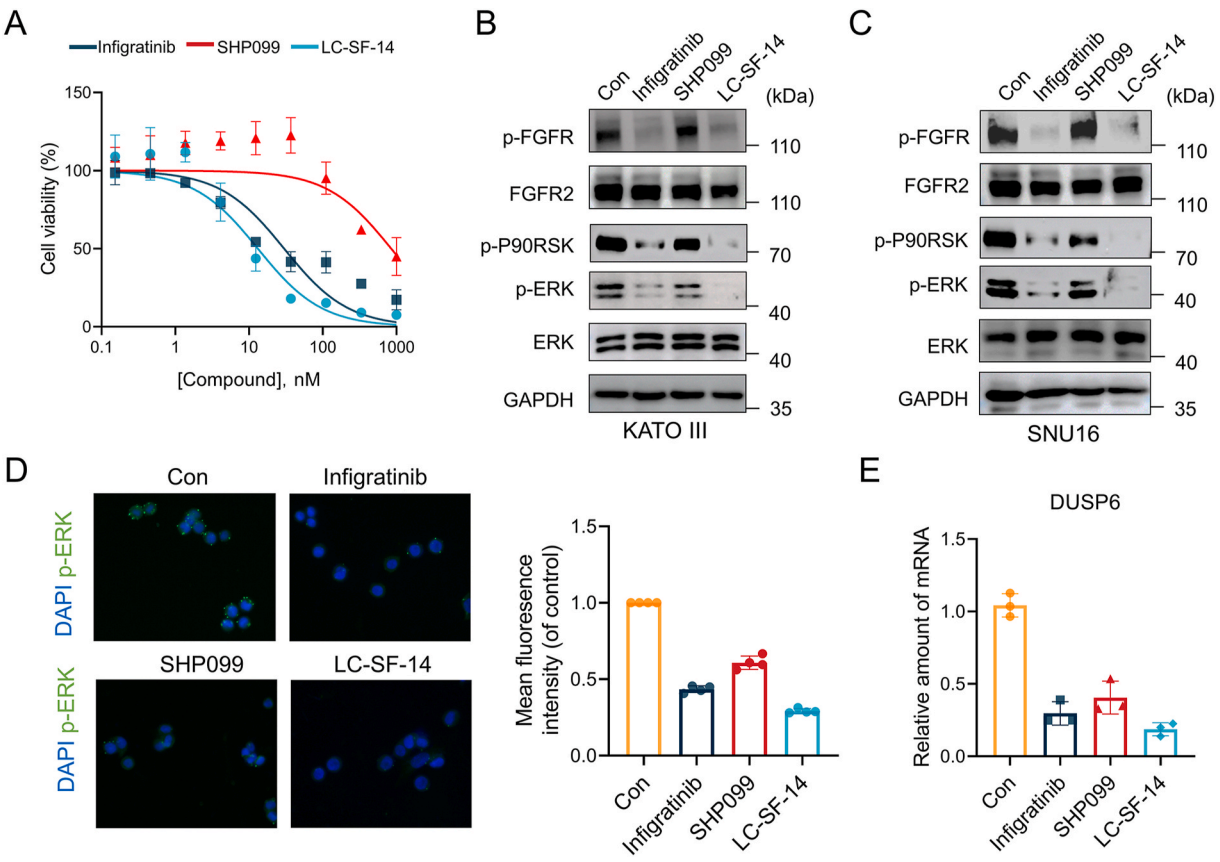

Fig. 4. LC-SF-14 inhibits the proliferation and FGFR2 signaling in cells. (A) Proliferation assay of LC-SF-14, infigratinib, or SHP099 on KATOIII cancer cells. (B–C) Levels of pFGFR, pERK, and pP90RSK in KATOIII (B) and SNU16 (C) cells after 12 h of incubation with infigratinib, SHP099 or LC-SF-14 at 20 nM (Experiments were performed in biological triplicates with similar results). (D) KATOIII cells treated with compound LC-SF-14, infigratinib, or SHP099 were stained with DAPI and p-ERK antibodies. (E) *DUSP6* mRNA expression in KATOIII cells treated with indicated compounds for 12 h.

4. Experimental section

4.1. Chemistry

The synthetic procedure and analytical data are as follows: Reagents and solvents were obtained from commercial suppliers and used without additional purification. The progress of all the reactions was routinely monitored using thin-layer chromatography (TLC) on silica gel GF254. The chromatographic column used for separation and purification contained 200–300 mesh silica gel powder supplied by Qingdao Ocean Corporation. The ^{1}H and ^{13}C NMR spectra were acquired on a Bruker 400 MHz spectrometer using DMSO-d_6 as the solvent. The ^{1}H NMR spectra were reported in parts per million (ppm) relative to tetramethylsilane (TMS), whereas the ^{13}C NMR spectra were reported in ppm with ^{1}H decoupling. In the presented spectral data, the format (δ) of chemical shift (multiplicity, J values in Hz, integration) was used, with abbreviations such as s (singlet), brs (broad singlet), d (doublet), t (triplet), q (quartet), and m (multiple). For electrospray ionization (ESI) mass spectrometry (MS), a Waters Alliance (e2695) equipped with a Q Da and PDA detector (2998) was used. High-resolution mass spectrometry (HRMS) was performed using an Agilent G6520 quadrupole time-of-flight mass spectrometer in the electrospray mode. The purity of all synthetic compounds was determined by HPLC analysis and found to be >95 %.

The synthetic approaches for the preparation of compounds **19a-19c** are outlined in Schemes 1. The synthesis of **12** began with an S_NAr reaction utilizing 2-chloro-3-fluoroaniline (**11**) and *tert*-butylthiol, facilitated by a base. Subsequently, the *tert*-butyl group was eliminated from compound **12** through a deprotection process using concentrated hydrochloric acid, resulting in intermediate **13**. The Cu(I)-catalyzed cross-coupling reaction between intermediate **13** and 3-bromo-6-chloropyrazin-2-amine (**14**) produced **15**. Compound **15** was then subjected to a reaction with *tert*-butyl (4-methylpiperidin-4-yl)carbamate in the presence of DIPEA as a base in DMSO at 100 °C for 6 h, yielding the key intermediate **16**. This intermediate further reacted with methyl 3-chloro-3-oxovalerate derivatives (**17a-17c**), which differed in carbon chain length. The final step involved hydrolysis of the methyl ester group to obtain the desired intermediates **19a-19c**.

Target compounds **1–8** were synthesized by the reaction of intermediates **24a-24d** with 4,6-dichloropyropyridine, as depicted in Schemes 2. For example, the combination of aromatic amines **21** and **22** with 4,6-dichloropyrimidine and methylamine, respectively, yielded intermediates **24a** and **24b**. These intermediates were then reacted with isocyanate, followed by treatment with TFA, to produce the desired intermediates **25a** and **25b**. Following this, intermediates **19a-19c** were combined with **25a** and **25b** and subjected to TFA treatment, resulting in the formation of target compounds **1–6**. Alternatively, the S_NAr reaction of aliphatic amines **23a** and **23b** with 4,6-dichloropyrimidine led to the formation of intermediates **24c** and **24d**. These intermediates underwent reaction with isocyanate and subsequent TFA treatment to yield intermediates **25c** and **25d**. Finally, the reaction of intermediate **19b** with **25c** and **25d**, followed by TFA treatment, led to the synthesis of the target compounds **7** and **8**.

As illustrated in Scheme 3, the preparation of compound **9** involved a series of chemical reactions. Initially, intermediates **16** and 16-(benzyloxy)-16-oxohexadecanoic acid (**26**) underwent amide condensation with TCFH and NMI as the coupling reagents. This step was achieved by adding NaOH to yield the intermediate **28**. Subsequently, intermediate

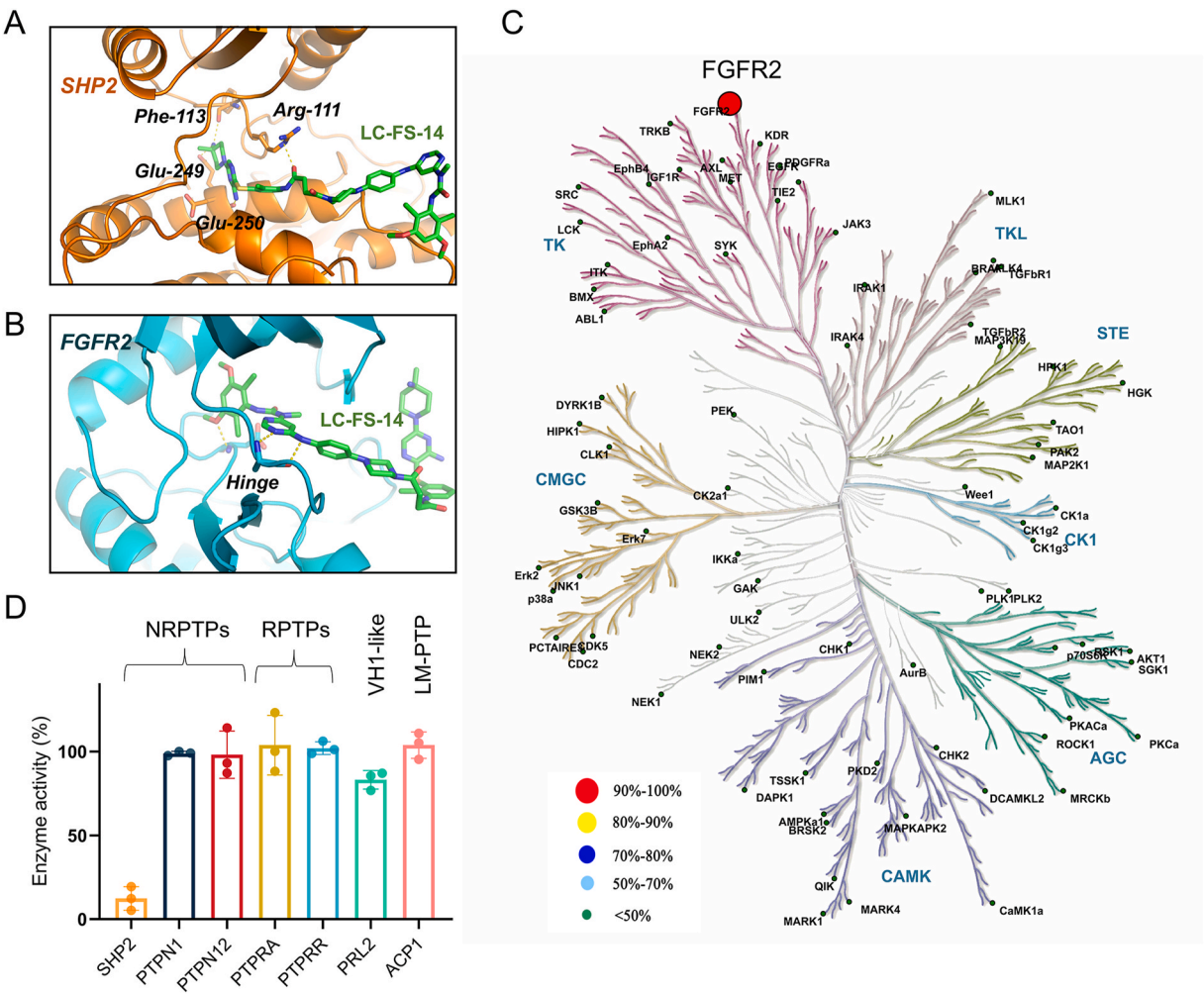

Fig. 5. LC-SF-14 selectivity target SHP2 and FGFR. (A) Predicted binding mode of compound LC-SF-14 with SHP2 tunnel site. (B) Predicted binding mode of LC-SF-14 with FGFR kinase domain. (C) Kinase selectivity profile of LC-SF-14 against 80 kinases assayed at the concentration of 1 μM. (D) Inhibitory activities of compound LC-SF-14 against representative mammalian PTPs from different subfamilies at 1 μM.

28 was combined with intermediate **25b**, which had been previously treated with TFA. This final reaction sequence resulted in the formation of target compound **9**.

The preparation of compound **10** is illustrated in Scheme 3. A key step involves the amide condensation of **16** with 12-(4-(((9H-fluoren-9-yl)methoxy)carbonyl)piperazin-1-yl)acetic acid (**29**), facilitated by TCFH and NMI as coupling agents. This reaction was followed by removal of the Fmoc protecting group, resulting in the formation of intermediate **31**. Subsequently, intermediate **31** underwent nucleophilic substitution with 11-bromoundecanoic acid, leading to the formation of intermediate **32**. The final step involved amide condensation between intermediate **32** and compound **25b**, followed by the removal of the Boc protecting group. These reactions culminated in the synthesis of compound **10**.

3-(*tert*-Butylthio)-2-chloroaniline (**12**).

To a solution of *tert*-butylthiol (23.5 mL, 18.7 g, 206.1 mmol, 3.0 equiv) and 2-chloro-3-fluoroaniline (10.0 g, 68.7 mmol, 1 equiv) in anhydrous DMF (80 mL), cesium carbonate (56.0 g, 171.8 mmol, 2.5 equiv) was added at rt. The reaction mixture was then heated to 120 °C and stirred for 36 h under a nitrogen atmosphere. After cooling, the reaction solution was extracted with NH_4Cl (100 ml) and EtOAc (60 mL × 3). The combined organic layers were washed with saline water and dried using Na_2SO_4. Removal of the volatiles under reduced pressure followed by flash chromatography purification resulted in an 89 % yield of compound **13**, which can be directly used for the next reaction.

3-Amino-2-chlorobenzenethiol Hydrochloride (**13**).

A concentrated hydrochloric acid solution (170 mL) was used to suspend 3-(*tert*-Butylthio)-2-chloroaniline (19.5 g, 90.4 mmol). The mixture was then heated and stirred at 80 °C for 6 h. After cooling, volatile compounds were eliminated by applying reduced pressure, and the white solid was washed with a mixed solution (30 mL, hydrochloric acid: *n*-hexane = 1:2) to give 3-amino-2-chlorophenylthiol hydrochloride (13.8 g, 73 %), which was then directly employed in the subsequent stage.

3-((3-Amino-2-chlorophenyl)thio)-6-chloropyrazin-2-amine (**15**).

K_3PO_4 (29.74 g, 140.1 mmol, 2.6 equiv), CuI (2.05 g, 10.8 mmol, 0.2 equiv), and 1,10-phenanthroline (3.89 g, 21.6 mmol, 0.4 equiv) were added to the dioxane (200 ml) solution of 3-bromo-6-chloropyrazin-2-amine (11.15 g, 53.9 mmol, 1 equiv) and 3-amino-2-chlorobenzenethiol hydrochloride (13.8 g, 70.05 mmol, 1.3 equiv). After degassing three times, stir the mixture at 90 °C in dry N_2 for 16 h. The reaction mixture was cooled to rt, dilute with EtOAc, and filtered through the Celite. Afterward, the solvent was removed under reduced pressure and purified by flash chromatography (n-hexane: EtOAc = 4:1) with a yield of 70 % to obtain 3-((3-Amino-2-chlorophenyl)thio)-6-chloropyrazin-2-amine as a yellow solid.

tert-Butyl (1-(6-amino-5-((3-amino-2-chlorophenyl)thio)pyrazin-2-yl)-4-methylpiperidin-4-yl (**16**).

A solution of compound **15** (10 g, 35.1 mmol, 1.0 equiv) and *tert*-butyl (4-methylpiperidin-4-yl) carbamate (13.1 mg, 61 mmol, 2.0 equiv)

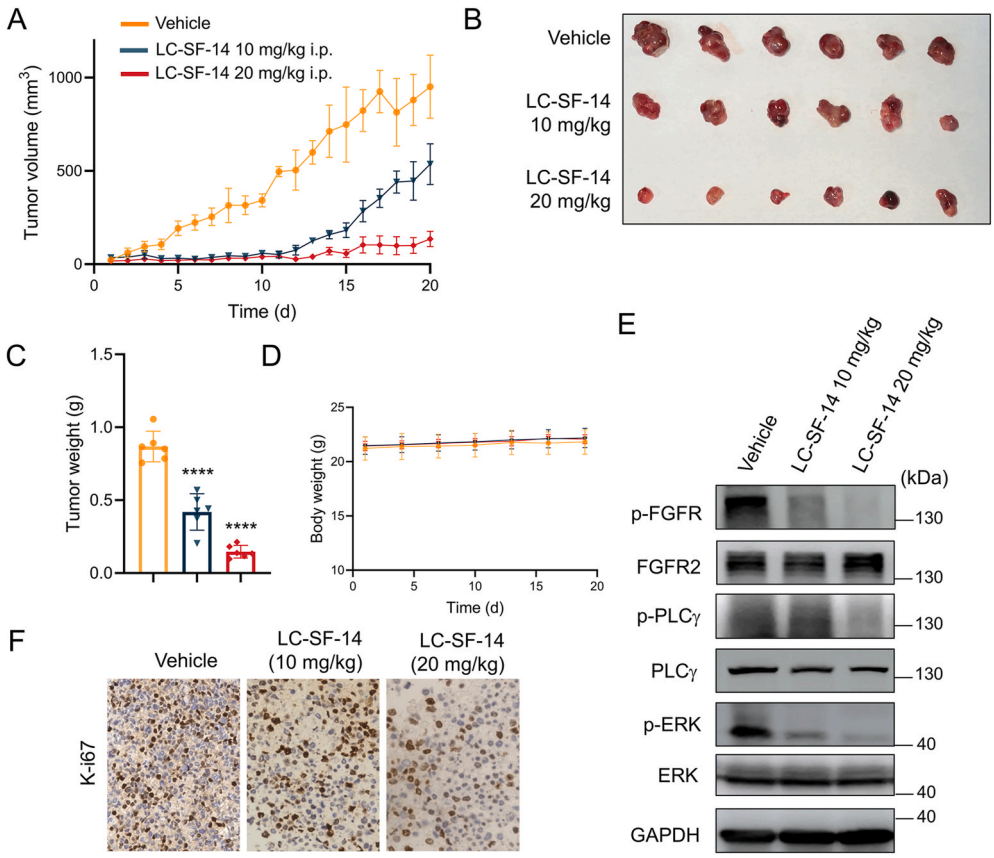

Fig. 6. Evaluation of LC-SF-14 *in vivo*. (A) Antitumor efficacy of LC-SF-14 in a SNU-16 xenograft model. Six SNU-16 tumor-bearing BALB/c nude mice were treated with vehicle or LC-SF-14 at 10 and 20 mg/kg/day. Tumor sizes were recorded every 2–3 days. (B) Tumor images of each group after LC-SF-14 (10 mg/kg), LC-SF-14 (20 mg/kg), or vehicle treatment. (C) Tumor weights in each group after treatment with vehicle or different dose of LC-SF-14. (E) Western blot analysis of tumor tissue lysates for the phosphorylation levels of FGFR, PLCγ, and Erk. (F) Representative images of immunohistochemical staining for Ki-67 in tumor tissues.

in DMSO (200 ml) was treated with DIPEA (30.5 ml, 175.5 mmol, 5.0 equiv). The resulting mixture was then heated at 100 °C for 6 h. After allowing the mixture to cool down to rt, it was poured into cold water containing saturated aqueous NH_4Cl (6.95 mol/l, 50 ml) and extracted with 100 ml of EtOAc three times. The combined organic layer was washed with water and saturated salt water, dried with Na_2SO_4, and subsequently evaporated under vacuum. The resulting residue was purified using flash chromatography (*n*-hexane: EtOAc = 4:1), obtaining compound **16** as a white solid with an 84 % yield.

Methyl 3-((3-((3-Amino-5-(4-((tert-butoxycarbonyl)amino)-4-methylpiperidin-1-yl)pyrazin-2-yl)thio)-2-chlorophenyl)amino)-3-oxopropanoate (**18a**).

A solution containing *tert*-butyl (1- (6-amino-5- ((3-amino-2-chlorophenyl) thio) pyrazine-2-yl) -4-methylpiperidine-4-yl) **16** (317 mg, 0.682 mmol, 1 equiv) and DIPEA (592.6 μl, 3.14 mmol, 5 equiv) in DCM (5 ml) was cooled to 0 °C. Methyl 3-chloro-3-oxopropionate (109.7 μl, 1.02 mmol, 1.5 equiv) was added dropwise and the mixture was stirred for 1 h. The reaction mixture was then warmed to rt and stirred for an additional 2 h before being poured into a solution of aq. $NaHCO_3$ (50 ml). After extraction with DCM (20 ml × 3), the combined organic layer was washed with saline, dried with Na_2SO_4, and evaporated under vacuum. The resulting residue was purified using flash chromatography (*n*-hexane: EtOAc = 4:1) to yield **18a** as a white solid with a 72 % yield.

3-((3-((3-Amino-5-(4-((tert-butoxycarbonyl)amino)-4-methylpiperidin- 1-yl)pyrazin-2-yl)thio)-2-chlorophenyl)amino)-3-oxopropanoic Acid (**19a**).

We added 80.5 mg (1.96 mmol, 4 equiv) of lithium hydroxide monohydrate to a solution of **18a** (277 mg, 0.49 mmol, 4 equiv) in a mixture of THF/MeOH/H_2O (3:2:1) at 0 °C and stirred it for 1 h. Then, the reaction mixture was heated to room temperature and stirred for 2 h. After quenching with a solution of 1.14 mol/l NH_4Cl to achieve pH~3, we extracted the resulting mixture with 20 ml of EtOAc three times. The organic layer was washed with saline, dried using anhydrous Na_2SO_4, and concentrated under reduced pressure. The obtained residue was further purified using flash chromatography (MeOH/DCM = 1:30), resulting in a yield of 85 % and obtaining compound **19a** as a white yellow solid.

tert-Butyl 4-(4-((6-(Methylamino)pyrimidin-4-yl)amino)phenyl) piperazine-1-carboxylate (**24a**).

IPA (8 ml) was mixed with DIPEA (3.2 ml, 18.42 mol, 3 equiv) and 4,6-Dichloropyrimidine (1 g, 6.76 mmol, 1.1 equiv). *tert*-Butyl 4-(4-aminophenyl)piperazine-1-carboxylate (1.7 g, 6.14 mmol, 1 equiv) dissolved in 7 ml of IPA was then added dropwise and further stirred at 40 °C for 16 h. The crude product, a white solid (1.92 g), was obtained by evaporating an appropriate amount of solvent and filtering, without needing any additional purification. In a separate reaction, DIPEA (2.8 ml, 15 mmol, 3 equiv) and methylamine (30 %wt 5 ml, 30 mmol, 6 equiv) were added to a 1-butanol solution of *tert*-Butyl 4-(4-((6-chloropyrimidin-4-yl)amino)phenyl)piperazine-1-carboxylate (1.92 g, 5 mmol, 1 equiv). The mixture was heated in a pressure tubing at 120 °C for 12 h. After cooling and evaporating the solvent, the product **24a** was obtained with a yield of 98 %.

tert-butyl (4-((6-(methylamino)pyrimidin-4-yl)amino)phenyl)carbamate (**24b**)

The preparation method of this compound is similar to that of compound **24a**, and the product was obtained with a yield of 87 %.

tert-butyl (2-((6-(methylamino)pyrimidin-4-yl)amino)ethyl)carbamate (**24c**)

The preparation method of this compound is similar to that of compound **24a**, and the product was obtained with a yield of 83 %.

tert-butyl (4-((6-(methylamino)pyrimidin-4-yl)amino)butyl)carbamate (**24d**)

The preparation method of this compound is similar to that of compound **24a**, and the product was obtained with a yield of 67 %.

3-(2,6-Dichloro-3,5-dimethoxyphenyl)-1-methyl-1-(6-((4-(piperazin-1-yl)phenyl)amino)pyrimidin-4-yl)urea (**25a**).

Triethylamine was added slowly to THF (40 ml) containing 2,6-Dichloro-3,5-dimethoxyaniline (888 mg, 4 mmol, 2 equiv) and triphosgene (593.4 g, 2 mmol, 1 equiv) at a temperature of −10 °C, under nitrogen protection. The temperature of the reaction gradually increased to rt, resulting in the formation of a white precipitate. The reaction was allowed to proceed for 1 h. The crude isocyanate obtained after heating to 80 °C and refluxing for 1 h was resuspended in toluene. To a mixture of toluene (60 ml) containing the isocyanates, *tert*-butyl 4-(4-((6-(methylamino)pyrimidin-4-yl)amino)phenyl)piperazine-1-carboxylate (1.54 g, 4 mmol, 2 equiv) and DIPEA (1.4 ml, 8 mmol, 4 equiv) were added, and the mixture was reacted at 80 °C for 18 h. The crude product was purified by flash chromatography (using DCM/MeOH in a ratio of 30:1) to yield a white solid (800 mg). *tert*-Butyl 4-(4-((6-(3-(2,6-dichloro-3,5-dimethoxyphenyl)-1,3-dimethylureido)pyrimidin-4-yl)amino)phenyl)piperazine-1-carboxylate (800 mg) was dissolved in a mixture of DCM/TFA (1:1, 10 ml) and stirred at rt for 2 h. The solvent was then evaporated, and the residue was dissolved in THF and stirred with saturated aqueous $NaHCO_3$ solution (1.54 mol/l) for 30 min. The resulting brown precipitate was filtered, washed with water, and dried to obtain **25a** as a yellow solid with a yield of 65 %.

1-(6-((4-aminophenyl)amino)pyrimidin-4-yl)-3-(2,6-dichloro-3,5-dimethoxyphenyl)-1-methylurea (**25b**)

The preparation method of this compound is similar to that of compound **25a**, and the product was obtained with a yield of 54 %.

1-(6-((2-aminoethyl)amino)pyrimidin-4-yl)-3-(2,6-dichloro-3,5-dimethoxyphenyl)-1-methylurea (**25c**)

The preparation method of this compound is similar to that of compound **25a**, and the product was obtained with a yield of 61 %.

1-(6-((3-aminopropyl)amino)pyrimidin-4-yl)-3-(2,6-dichloro-3,5-dimethoxyphenyl)-1-methylurea (**25d**)

The preparation method of this compound is similar to that of compound **25a**, and the product was obtained with a yield of 46 %.

N-(3-((3-amino-5-(4-amino-4-methylpiperidin-1-yl)pyrazin-2-yl)thio)-2-chlorophenyl)-3-(4-(4-((6-(3-(2,6-dichloro-3,5-dimethoxyphenyl)-1-methylureido)pyrimidin-4-yl)amino)phenyl)piperazin-1-yl)-3-oxopropanamide (**1**)

A solution of **25a** (69.76 mg, 0.131 mmol, 1 equiv) was introduced to a solution containing **19a** (72.2 mg, 0.131 mmol,1 equiv) in DIPEA (114 l, 0.655 mmol, 5 equiv) and DMF (2 ml). Following that, HATU (54.80 mg, 0.144 mmol, 1.1 equiv) was added and the reaction mixture was stirred at rt for 1 h. Afterward, the mixture was poured into cold water (10 ml) and extracted with EtOAc (5 ml × 3). The combined organic layer was washed with water and salt water, dried with Na_2SO_4, and then evaporated under vacuum. The resulting residue was dissolved in DCM (3 ml) and treated with TFA (1 ml) at 0 °C. The final product was purified using flash chromatography (DCM/MeOH = 10:1) to obtain the compound **1** a yield of 43 %. ^{1}H NMR (400 MHz, DMSO-d_6) δ 12.10 (s, 1H), 10.21 (s, 1H), 9.58 (s, 1H), 8.41 (s, 1H), 7.66 (d, J = 4.4 Hz, 2H), 7.47 (d, J = 8.4 Hz, 2H), 7.18 (t, J = 8.1 Hz, 1H), 7.03–6.94 (m, 2H), 6.90 (s, 1H), 6.51–6.40 (m, 2H), 6.19 (s, 2H), 3.94 (s, 6H), 3.87–3.81 (m, 2H), 3.66 (q, J = 5.3, 4.8 Hz, 4H), 3.48 (dt, J = 13.1, 5.8 Hz, 2H), 3.32 (s, 3H), 3.12 (dt, J = 25.9, 5.1 Hz, 4H), 2.51–2.46 (m, 4H), 1.64 (d, J = 6.6 Hz, 4H), 1.28 (s, 3H). ^{13}C NMR (101 MHz, DMSO) δ 166.37, 162.15, 159.62, 156.32, 154.69, 154.09, 153.33, 147.30, 137.99, 136.15, 135.00, 127.60, 122.62, 122.34, 121.65, 120.78, 117.01, 113.49, 113.04, 97.04, 57.17, 50.63, 49.64, 49.26, 46.09, 45.84, 41.81, 41.62, 40.55, 40.34, 40.13, 39.92, 39.71, 39.50, 39.30, 36.30, 32.17, 25.64, 11.78. ESI-HRMS: *m/z* 964.2759 [M +H] + (calcd for $C_{43}H_{48}Cl_3N_{13}O_5S$, 964.2760).

N-(3-((3-amino-5-(4-amino-4-methylpiperidin-1-yl)pyrazin-2-yl)thio)-2-chlorophenyl)-4-(4-(4-((6-(3-(2,6-dichloro-3,5-dimethoxyphenyl)-1-methylureido)pyrimidin-4-yl)amino)phenyl)piperazin-1-yl)-4-oxobutanamide (**2**)

The preparation method of this compound is similar to that of compound **1**, and the product was obtained with a yield of 53 %. ^{1}H NMR (400 MHz, DMSO-d_6) δ 12.05 (s, 1H), 9.54 (d, J = 23.1 Hz, 2H), 8.39 (s, 1H), 7.63 (s, 1H), 7.45 (d, J = 8.6 Hz, 2H), 7.33 (t, J = 8.0 Hz, 1H), 7.15–7.12 (m, 1H), 6.97–6.94 (m, 2H), 6.90 (s, 2H), 6.45–6.40 (m, 2H), 6.23 (s, 1H), 3.94 (s, 6H), 3.71 (dd, J = 13.4, 5.6 Hz, 4H), 3.57 (d, J = 3.9 Hz, 4H), 3.30 (s, 3H), 3.13–3.10 (m, 2H), 3.04 (d, J = 5.3 Hz, 2H), 2.91–2.86 (m, 2H), 2.68 (t, J = 3.6 Hz, 2H), 1.85 (s, 2H), 1.53 (d, J = 6.0 Hz, 4H), 1.19 (s, 3H). ^{13}C NMR (101 MHz, DMSO) δ 176.18, 169.83, 168.96, 161.75, 159.23, 156.17, 155.96, 155.88, 154.28, 153.78, 153.70, 152.91, 147.01, 138.74, 136.00, 134.59, 131.57, 127.81, 126.99, 121.95, 120.65, 120.36, 116.57, 112.87, 112.65, 111.98, 96.67, 56.75, 49.28, 49.09, 48.92, 41.12, 36.87, 31.76, 28.71, 27.67, 26.84. ESI-HRMS: *m/z* 978.2909 [M +H] + (calcd for $C_{44}H_{50}Cl_3N_{13}O_5S$, 978.2917).

N-(3-((3-amino-5-(4-amino-4-methylpiperidin-1-yl)pyrazin-2-yl)thio)-2-chlorophenyl)-5-(4-(4-((6-(3-(2,6-dichloro-3,5-dimethoxyphenyl)-1-methylureido)pyrimidin-4-yl)amino)phenyl)piperazin-1-yl)-5-oxopentanamide (**3**)

The preparation method of this compound is similar to that of compound **1**, and the product was obtained with a yield of 47 %. ^{1}H NMR (400 MHz, DMSO-d_6) δ 12.05 (s, 1H), 9.53 (d, J = 22.5 Hz, 2H), 8.40 (s, 1H), 7.64 (s, 1H), 7.45 (d, J = 8.6 Hz, 2H), 7.43–7.39 (m, 1H), 7.16 (t, J = 8.0 Hz, 1H), 6.99–6.88 (m, 4H), 6.46–6.41 (m, 2H), 6.14 (s, 1H), 3.94 (s, 6H), 3.76–3.68 (m, 4H), 3.54 (dd, J = 14.2, 9.1 Hz, 4H), 3.31 (s, 3H), 3.10 (d, J = 5.4 Hz, 2H), 3.06 (d, J = 5.2 Hz, 2H), 2.47–2.41 (m, 4H), 1.88 (s, 1H), 1.84 (t, J = 7.5 Hz, 2H), 1.54 (t, J = 5.7 Hz, 3H), 1.23 (s, 2H), 1.20 (s, 3H). ^{13}C NMR (101 MHz, DMSO) δ 170.31, 162.95, 158.97, 155.90, 154.28, 153.70, 152.92, 135.91, 134.59, 121.94, 120.38, 116.58, 112.99, 112.65, 97.96, 56.76, 49.17, 48.93, 44.95, 40.92, 36.78, 31.76, 31.59, 21.85, 20.90, 20.86. ESI-HRMS: *m/z* 992.3068 [M +H] + (calcd for $C_{45}H_{52}Cl_3N_{13}O_5S$, 992.3073).

N^1-(3-((3-amino-5-(4-amino-4-methylpiperidin-1-yl)pyrazin-2-yl)thio)-2-chlorophenyl)-N^3-(4-((6-(3-(2,6-dichloro-3,5-dimethoxyphenyl)-1-methylureido)pyrimidin-4-yl)amino)phenyl)malonamide (**4**)

The preparation method of this compound is similar to that of compound **1**, and the product was obtained with a yield of 63 %. ^{1}H NMR (400 MHz, DMSO-d_6) δ 12.00 (s, 1H), 10.26 (s, 1H), 10.09 (s, 1H), 9.69 (s, 1H), 8.45 (s, 1H), 7.71 (d, J = 8.0 Hz, 1H), 7.64 (s, 1H), 7.58 (s, 4H), 7.19 (t, J = 8.0 Hz, 1H), 6.91 (s, 1H), 6.51 (s, 1H), 6.43 (dd, J = 7.9, 1.4 Hz, 1H), 6.14 (s, 2H), 5.76 (s, 1H), 3.94 (s, 6H), 3.76–3.70 (m, 2H), 3.62 (s, 2H), 3.57 (d, J = 6.6 Hz, 2H), 1.55 (t, J = 5.6 Hz, 4H), 1.23 (s, 2H), 1.20 (s, 3H). ^{13}C NMR (101 MHz, DMSO) δ 165.73, 165.67, 161.57, 159.32, 155.98, 155.89, 154.30, 153.70, 152.92, 137.61, 135.65, 135.37, 134.57, 133.88, 127.25, 121.84, 120.78, 120.38, 119.99, 113.01, 112.68, 96.70, 90.64, 56.77, 54.98, 49.75, 44.62, 36.37, 31.82, 29.10, 25.88. ESI-HRMS: *m/z* 895.2184 [M +H] + (calcd for $C_{39}H_{41}Cl_3N_{12}O_5$ S, 895.2182).

N^1-(3-((3-amino-5-(4-amino-4-methylpiperidin-1-yl)pyrazin-2-yl)thio)-2-chlorophenyl)-N^4-(4-((6-(3-(2,6-dichloro-3,5-dimethoxyphenyl)-1-methylureido)pyrimidin-4-yl)amino)phenyl)succinimide (**5**)

The preparation method of this compound is similar to that of compound **1**, and the product was obtained with a yield of 28 %. ^{1}H NMR (400 MHz, DMSO-d_6) δ 12.04 (s, 1H), 10.01 (s, 1H), 9.65 (d, J = 13.2 Hz, 2H), 8.44 (d, J = 0.8 Hz, 1H), 7.64 (s, 1H), 7.57 (t, J = 7.7 Hz, 4H), 7.49–7.44 (m, 1H), 7.16 (t, J = 8.0 Hz, 1H), 6.90 (s, 1H), 6.50 (s, 1H), 6.43 (dd, J = 8.0, 1.5 Hz, 1H), 6.12 (s, 2H), 3.94 (s, 6H), 3.71–3.66 (m, 2H), 3.63 (d, J = 5.6 Hz, 2H), 3.58 (d, J = 5.3 Hz, 2H), 3.33 (s, 3H), 2.74 (d, J = 9.3 Hz, 2H), 2.66 (d, J = 6.7 Hz, 2H), 1.52 (t, J = 5.7 Hz,

4H), 1.18 (s, 3H). ^{13}C NMR (101 MHz, DMSO) δ 170.87, 169.99, 161.59, 159.27, 155.89, 154.27, 153.71, 152.89, 137.57, 135.91, 134.65, 134.56, 127.01, 122.37, 120.83, 120.36, 119.54, 112.81, 112.66, 96.98, 56.75, 48.58, 40.14, 39.93, 39.73, 39.52, 39.31, 39.10, 38.89, 37.40, 31.78, 31.36, 31.20, 30.92, 30.72, 28.70, 27.87. ESI-HRMS: *m/z* 909.2342 [M +H] + (calcd for $C_{40}H_{43}Cl_3N_{12}O_5S$, 909.2338).

N^{1}-(3-((3-amino-5-(4-amino-4-methylpiperidin-1-yl)pyrazin-2-yl) thio)-2-chlorophenyl)-*N*^{5}-(4-((6-(3-(2,6-dichloro-3,5-dimethoxyphenyl)-1-methylureido)pyrimidin-4-yl)amino)phenyl)glutaramide (**6**)

The preparation method of this compound is similar to that of compound **1**, and the product was obtained with a yield of 25 %. ^{1}H NMR (400 MHz, DMSO-d_6) δ 12.02 (s, 1H), 9.93 (s, 1H), 9.62 (d, J = 31.1 Hz, 2H), 8.44 (s, 1H), 7.63 (s, 1H), 7.56 (q, J = 9.1 Hz, 4H), 7.44 (dd, J = 8.0, 1.5 Hz, 1H), 7.17 (t, J = 8.0 Hz, 1H), 6.90 (s, 1H), 6.50 (s, 1H), 6.45 (dd, J = 8.0, 1.5 Hz, 1H), 6.10 (s, 2H), 3.94 (s, 6H), 3.71 (dt, J = 13.5, 4.9 Hz, 2H), 3.55 (td, J = 8.3, 3.9 Hz, 2H), 3.33 (s, 3H), 3.28 (s, 2H), 2.46 (t, J = 7.2 Hz, 2H), 2.39 (t, J = 7.4 Hz, 2H), 1.93 (q, J = 7.3 Hz, 2H), 1.44 (q, J = 5.0 Hz, 4H), 1.10 (s, 3H). ^{13}C NMR (101 MHz, DMSO) δ 171.24, 170.53, 161.60, 159.29, 155.92, 154.29, 153.77, 152.91, 137.65, 135.89, 134.70, 134.57, 127.00, 124.04, 123.36, 122.63, 120.82, 120.39, 119.68, 112.68, 112.49, 97.76, 90.16, 56.76, 47.35, 40.39, 40.20, 40.15, 39.99, 39.94, 39.78, 39.73, 39.57, 39.52, 39.36, 39.31, 39.10, 38.89, 38.52, 35.50, 35.02, 31.79, 29.96, 27.99, 21.14. ESI-HRMS: *m/z* 923.2507 [M +H] + (calcd for $C_{41}H_{46}Cl_3N_{12}O_5S$, 923.2495).

N^{1}-(3-((3-amino-5-(4-amino-4-methylpiperidin-1-yl)pyrazin-2-yl) thio)-2-chlorophenyl)-*N*^{4}-(2-((6-(3-(2,6-dichloro-3,5-dimethoxyphenyl)-1-methylureido)pyrimidin-4-yl)amino)ethyl)succinimide (**7**)

The preparation method of this compound is similar to that of compound **1**, and the product was obtained with a yield of 33 %. ^{1}H NMR (400 MHz, DMSO-d_6) δ 12.23 (s, 1H), 9.60 (s, 1H), 8.30 (s, 1H), 8.06 (s, 4H), 7.67 (s, 1H), 7.63 (s, 1H), 7.46 (dd, J = 8.1, 1.5 Hz, 1H), 7.15 (t, J = 8.0 Hz, 1H), 6.89 (s, 1H), 6.43 (dd, J = 8.0, 1.5 Hz, 1H), 6.20 (s, 2H), 3.94 (s, 9H), 3.28 (ddd, J = 25.2, 16.4, 6.0 Hz, 8H), 2.64 (t, J = 7.0 Hz, 2H), 2.42 (t, J = 7.3 Hz, 2H), 1.73 (t, J = 6.1 Hz, 4H), 1.38 (s, 3H). ^{13}C NMR (101 MHz, DMSO) δ 172.06, 170.99, 163.48, 158.57, 158.23, 155.85, 154.29, 153.60, 152.95, 137.35, 135.97, 134.62, 127.02, 122.53, 120.36, 113.73, 112.60, 96.61, 56.75, 52.06, 34.17, 31.81, 30.51, 22.01. ESI-HRMS: *m/z* 861.2347 [M +H] + (calcd for $C_{36}H_{43}Cl_3N_{12}O_5S$, 861.2338).

N^{1}-(3-((3-amino-5-(4-amino-4-methylpiperidin-1-yl)pyrazin-2-yl) thio)-2-chlorophenyl)-*N*^{4}-(4-((6-(3-(2,6-dichloro-3,5-dimethoxyphenyl)-1-methylureido)pyrimidin-4-yl)amino)butyl)succinimide (**8**)

The preparation method of this compound is similar to that of compound **1**, and the product was obtained with a yield of 42 %. ^{1}H NMR (400 MHz, DMSO-d_6) δ 12.34 (s, 1H), 9.60 (s, 1H), 8.27 (s, 1H), 7.96 (q, J = 7.4, 5.7 Hz, 1H), 7.62 (s, 2H), 7.43 (t, J = 6.4 Hz, 1H), 7.14 (td, J = 8.0, 3.2 Hz, 1H), 6.89 (s, 1H), 6.42 (dd, J = 7.9, 1.5 Hz, 1H), 6.18 (s, 1H), 6.08 (s, 2H), 3.93 (s, 6H), 3.76–3.70 (m, 2H), 3.52 (t, J = 4.8 Hz, 2H), 3.26 (s, 4H), 3.17 (s, 1H), 3.10–3.05 (m, 2H), 2.89 (s, 2H), 2.82 (s, 1H), 2.68 (dd, J = 4.4, 2.7 Hz, 2H), 2.62 (d, J = 2.6 Hz, 2H), 2.40 (t, J = 7.3 Hz, 2H), 2.34 (p, J = 1.5 Hz, 1H), 1.47–1.43 (m, 4H), 1.09 (s, 3H). ^{13}C NMR (101 MHz, DMSO) δ 172.12, 171.09, 163.73, 158.97, 158.66, 158.35, 158.04, 155.99, 154.36, 153.85, 153.05, 142.61, 138.08, 136.02, 134.75, 127.07, 121.82, 118.84, 115.87, 112.89, 112.63, 79.37, 56.83, 56.18, 48.34, 47.78, 38.35, 38.25, 30.61, 26.75. ESI-HRMS: *m/z* 889.2654 [M +H] + (calcd for $C_{36}H_{43}Cl_3N_{12}O_5S$, 889.2651).

16-((3-((3-Amino-5-(4-((tert-butoxycarbonyl)amino)-4-methylpiperidin-1-yl)pyrazin-2-yl)thio)-2-chlorophenyl)amino)-16-oxohexadecanoic Acid (**28**).

TCFH (432.23 mg, 1.54 mmol, 1.3 equiv) was added to MeCN/THF (1: 1, 7 ml) at room temperature, along with **16** (550 mg, 1.185 mmol, 1 equiv),16-(benzyloxy)-16-oxohexadecanoic acid (535.04 mg, 1.422 mmol, 1.2 equiv), and NMI (340.51 mg, 4.15 mmol, 3.5 equiv), and stirred for 3 h. Afterward, the resulting mixture was poured into cold water (210 ml) and extracted with EtOAc (20 ml × 3). The combined organic layer was washed with water and saline solution, dried with Na_2SO_4, and evaporated under vacuum to obtain crude **27**, which was directly used in the next step. The crude **27** was dissolved in MeOH/THF/H_2O (2:1:1,8 ml), and NaOH was added. The mixture was stirred at room temperature for 8 h. The pH was adjusted to 6 and then diluted with EtOAc (30 ml) and water (30 ml). The combined organic layer was washed with water and saline solution, dried with Na_2SO_4, and evaporated under vacuum. The resulting residue was purified by flash chromatography (DCM/MeOH = 30:1), yielding **28** as a white solid with a yield of 26 %.

N^{1}-(3-((3-amino-5-(4-amino-4-methylpiperidin-1-yl)pyrazin-2-yl) thio)-2-chlorophenyl)-*N*^{16}-(4-((6-(3-(2,6-dichloro-3,5-dimethoxyphenyl)-1-methylureido)pyrimidin-4-yl)amino)phenyl)hexadecanediamide (**9**)

A solution of **25a** (100 mg,0.216 mmol,1 equiv) was combined with a solution of 16-((3-((3-Amino-5-(4-((tert-butoxycarbonyl)amino)-4-methylpiperidin-1-yl)pyrazin-2-yl)thio)-2-chlorophenyl)amino)-16-oxohexadecanoic Acid (158.49 mg, 0.216 mmol, 1 equiv) in DIPEA (139.58 μl,1.08 mmol,5 equiv) and DMF (3 ml). HATU (90 mg, 0.23 mmol, 1.1 equiv) was subsequently added, and the mixture was stirred at rt for 1 h. The resulting mixture was then added to cold water (80 ml) and extracted with EtOAc (20 ml × 3). The combined organic layer was washed with water and salt water, dried with Na_2SO_4, and evaporated under a vacuum. The resulting residue was dissolved in DCM (3 ml), and TFA (1 ml) was added at 0 °C. The compound was further purified using flash chromatography (DCM/MeOH = 10:1) to yield compound **9** with 17 % yield. ^{1}H NMR (400 MHz, DMSO-d_6) δ 12.02 (s, 1H), 9.84 (s, 1H), 9.63 (s, 1H), 9.49 (s, 1H), 8.43 (s, 1H), 7.64 (s, 1H), 7.59–7.49 (m, 4H), 7.40 (d, J = 7.9 Hz, 1H), 7.15 (t, J = 8.0 Hz, 1H), 6.91 (s, 1H), 6.48 (s, 1H), 6.43 (d, J = 8.0 Hz, 1H), 6.13 (s, 2H), 3.94 (s, 6H), 3.79–3.72 (m, 2H), 3.53 (s, 2H), 3.32 (s, 3H), 2.39–2.33 (m, 2H), 2.27 (t, J = 7.4 Hz, 2H), 1.57 (q, J = 6.7, 5.6 Hz, 8H), 1.27 (d, J = 12.5 Hz, 25H). ^{13}C NMR (101 MHz, DMSO) δ 172.20, 171.28, 161.05, 158.69, 156.26, 154.31, 153.11, 138.15, 136.49, 134.68, 127.05, 120.80, 119.65, 112.68, 56.78, 36.79, 36.40, 36.29, 36.08, 31.81, 31.58, 29.13, 28.90, 28.78, 28.67, 25.27. ESI-HRMS: *m/z* 1077.4220 [M +H] + (calcd for $C_{52}H_{64}Cl_3N_{12}O_5S$, 1077.4216).

tert-Butyl (1-(6-Amino-5-((2-chloro-3-(2-(piperazin-1-yl)- acetamido) phenyl)thio)pyrazin-2-yl)-4-methylpiperidin-4-yl)-carbamate (**31**). TCFH (214.87 mg, 0.766 mmol, 1.3 equiv) was added to a mixture of MeCN/THF (1:1, 6 ml) containing **16** (247 mg, 0.532 mmol, 1 equiv), 2-(4-(((9H-fluoren-9-yl)methoxy)carbonyl)piperazin-1-yl)acetic acid (246 mg, 0.672 mmol, 1.1 equiv), and NMI (174.86 mg, 2.13 mmol, 3.5 equiv) at rt. The mixture was stirred for 6 h. Then, the reaction mixture was mixed with cold water (30 ml) and the resulting solution was extracted with EtOAc (30 ml). The combined organic layer was washed with water and salt water, and dried with Na_2SO_4. The solvent was evaporated under vacuum, resulting in crude **30**, which was directly used in the next step. The crude **30** was dissolved in piperidine (2 ml) and MeCN (10 ml), and stirred at rt for 2 h. The solvent was then diluted with EtOAc (30 ml) and water (50 ml). The combined organic layer was washed with water and salt water, and dried with Na_2SO_4. The solvent was evaporated under a vacuum. The residue was purified using flash chromatography (DCM/MeOH = 30:1) to obtain **31** (144 mg, 48 % yield) as a white solid.

11-(4-(2-((3-((3-Amino-5-(4-((tert-butoxycarbonyl)amino)-4methylpiperidin-1-yl)pyrazin-2-yl)thio)-2-chlorophenyl)amino)-2oxoethyl) piperazin-1-yl)undecanoic Acid (**32**).

K_2CO_3 (3.0 equiv) and KI (1.2 equiv) were introduced to a solution containing the intermediate compound **31** (118 mg, 0.2 mmol) and 11-bromoundecanoic acid (1.2 equiv), all dissolved in DMF (5.0 mL). The reaction mixture was agitated for a duration of 12 h at a temperature of 60 °C. Subsequently, the reaction was diluted with the addition of EtOAc (30 mL) and water (30 mL). The layers were separated and washed with water, followed by drying over anhydrous Na_2SO_4 to remove residual moisture. The solution was filtered to remove the drying agent, and the

filtrate was subjected to concentration under reduced pressure. The resulting residue was subjected by pre-HPLC to yield the desired product **32** as a white solid, with an obtained mass of 71 mg and a yield of 46 %.

11-(4-(2-((3-((3-amino-5-(4-amino-4-methylpiperidin-1-yl)pyrazin-2-yl)thio)-2-chlorophenyl)amino)-2-oxoethyl)piperazin-1-yl)-*N*-(4-((6-(3-(2,6-dichloro-3,5-dimethoxyphenyl)-1-methylureido)pyrimidin-4-yl)amino)phenyl)undecanamide (**10**)

A solution of 11-(4-(2-((3-((3-Amino-5-(4-((tert-butoxycarbonyl)amino)-4-methylpiperidin-1-yl)pyrazin-2-yl)thio)-2-chlorophenyl)amino)-2-oxoethyl)piperazin-1-yl)undecanoic Acid (37 mg,0.0478 mmol, 1 equiv) in DIPEA (41,5 μl, 0.239 mmol, 5 equiv) and DMF (2 ml) was treated with **25a** (22.07 mg, 0.0478 mmol, 1 equiv). HATU (20 mg, 0.0517 mmol, 1.1 equiv) was then added, and the reaction mixture was stirred at room temperature for 1 h. The resulting mixture was poured into 60 ml of cold water and extracted with 20 ml of EtOAc. The combined organic layer was washed with water and saline solution, dried with Na_2SO_4, and evaporated under vacuum. The residue was dissolved in 3 ml of DCM and treated with 1 ml of TFA at 0 °C. Finally, compound **10** was obtained with a yield of 27 % by purifying the mixture through flash chromatography using DCM/MeOH as the solvent in a ratio of 10:1.^{1}H NMR (400 MHz, DMSO-d_6) δ 12.03 (s, 1H), 10.00 (s, 1H), 9.87 (s, 1H), 9.66 (s, 1H), 8.43 (s, 1H), 8.04 (dd, J = 8.3, 1.5 Hz, 1H), 7.61 (s, 1H), 7.58–7.51 (m, 4H), 7.19 (t, J = 8.1 Hz, 1H), 6.90 (s, 1H), 6.50 (s, 1H), 6.39 (dd, J = 8.0, 1.5 Hz, 1H), 6.08 (s, 2H), 3.94 (s, 6H), 3.73 (dd, J = 11.7, 6.6 Hz, 2H), 3.52 (dd, J = 8.9, 4.2 Hz, 2H), 3.32 (s, 2H), 3.16 (s, 3H), 2.67 (dt, J = 3.6, 1.8 Hz, 1H), 2.33 (dt, J = 3.6, 1.8 Hz, 1H), 2.30–2.24 (m, 5H), 1.60–1.56 (m, 2H), 1.42 (dt, J = 8.3, 4.6 Hz, 7H), 1.25 (d, J = 11.4 Hz, 18H), 1.08 (s, 3H). ^{13}C NMR (101 MHz, DMSO) δ 171.09, 168.60, 158.36, 158.06, 157.75, 155.93, 154.32, 153.85, 152.94, 137.68, 135.19, 121.84, 120.39, 119.65, 118.86, 115.88, 112.67, 112.13, 79.28, 57.91, 56.79, 53.15, 52.92, 47.14, 40.20, 40.14, 39.99, 39.94, 39.78, 39.73, 39.57, 39.52, 39.36, 39.31, 39.10, 38.89, 36.40, 31.81, 30.37, 29.09, 29.05, 29.03, 28.88, 28.77, 27.03, 26.41, 25.27, 24.60. ESI-HRMS: *m/z* 1119.4447 [M +H] + (calcd for $C_{53}H_{70}Cl_3N_{14}O_5S$, 1119.4434).

4.2. Protein expression

FGFR2 Kinase domain (P458-E768) was cloned to pET28a, with a cleavable N-terminal 8xHis tag. Kinase was co-expression with YopH in the *E. coli*. The protein was purified using His FF, HiTrap Q and Superdex 75 colums. The N-terminal His tag was cleaved by TEV protease after 1st round purification, and the protein was purified via 2nd affinity chromatography. The *PTPN11* gene encodes the full-length SHP2 was cloned into the pET30 vector and expressed in BL21 (DE3) *E. coli* cells. The cell lysis purified by Ni-NTA gravity column, HiTrap Q anion-exchange column and followed by size-exclusion chromatography. The purified SHP2 proteins were fast frozen and stored at −80 °C until further use.

4.3. Cell culture

The KATO III and SNU16 gastric cancer cell lines were kindly provided by the Cell Bank of the Chinese Academy of Sciences. KATO III and SNU16 cells were cultured in RPMI-1640 (BC-M-017) supplemented with 10 % FBS (Cat. BC-SE-FBS07, Bio-Channel) and 1 % penicillin/streptomycin (Cat. BL505A; Biosharp), and cells were cultured at 37 °C with 5 % CO_2.

4.4. Western blot assay

Cells were lysed to obtain proteins, followed by a centrifugation process at 12,000 rpm for a span of 10 min at 4 °C. The supernatant was carefully separated and the protein concentration of each sample was determined using the Rapid Gold BCA Protein Assay (Cat. A55861, ThermoFisher). The protein levels of all samples were regulated to ensure uniformity. Proteins were denatured using heat at a temperature of 100 °C for a duration of 10 min upon mixture with 5x protein loading buffer. The prepared samples were then segregated on SDS-PAGE and transferred to polyvinylidene difluoride (PVDF) membranes. These membranes underwent incubation at 4 °C overnight with primary antibody, diluted in a 5 % BSA-buffered TBST. The attached antibodies were visualized using a SuperPico ECL Chemiluminescence Kit (Cat. P10300A; Vazyme Biotech), and subsequent images were captured using the Vilber Fusion FX system.

The following primary antibodies were used: anti-phosphorylated fibroblast growth factor receptor (p-FGFR; Tyr653/654) (1:1000; cat. #3476), anti-FGFR2 (1:1000, Cat. #11835), anti-PLCγ1 antibody (1:1000, Cat. #5690). These were purchased from Cell Signaling Technology. The anti-p-ERK1/2(Thr202/Tyr204) (1:2000, Cat. ET1610-13), anti-ERK1/2 (1:2000, Cat. ET1601-29), and anti-GAPDH (1:2000, Cat. ET1601-4) antibodies were purchased from Huabio. The anti-p-PLCγ1 (Tyr783) antibody (1:1000, Cat# AF3210) and HRP-conjugated goat anti-rabbit IgG secondary antibodies (1:100000, Cat. No. HA1001) were purchased from Affinity Biosciences.

4.5. DiFMUP assay

Classical phosphatase substrate DiFMUP (Cat. D6567, Thermo Fisher Scientific) was used to evaluate SHP2 enzyme activity using a fluorescence assay. A fluorescence assay was performed in a 384-well plate (cat. #781086, Griener). The compounds were diluted with dimethyl sulfoxide to a concentration of 10 mM. Three variants of protein, SHP2-FL, SHP2-PTP, and SHP2$^{T253M/Q257L}$, all at 0.5 nM, were mixed with 5 μL of the test compounds in varied proportions along with an added 0.5 μM of pIRS-1 peptide. This particular peptide was procured from China-Peptides Company based in Shanghai, possessing a purity level exceeding 97 %. After a co-incubation period of 0.5 h, DiFMUP was added to initiate the reaction, which was then left at room temperature for 30 min. The reaction was halted by introducing the reaction stop reagent bpV(Phen). The measurement data were captured using a plate reader (SpectraMax iD5, Molecular Devices) at excitation and emission wavelengths of 340 and 450 nm, respectively.

4.6. BLI assay

For the binding assay of the formation of the ternary complex, we used the Octet Red 96 system (ForteBio). Biotinylated FGFR2 proteins were diluted to 1.10 μg ml^{-1} in Octet buffer (25 mM HEPES pH 8.0, 150 mM NaCl, 0.02 % Tween-20 and 0.02 % BSA). Sample were loaded onto Super streptavidin biosensors (ForteBio, 18–5057) for 160 s, washed in the Octet buffer for 300 s, quenched with 6.25 μM d-biotin for 100 s, and washed in the Octet buffer for 300 s. Washed biosensor were dipped in 10 μM LC-SF-14 for 150 s, and then washed in the Octet buffer for 300s. Finally, generated binary complexes were immersed in the SHP2 protein (1.10 μg ml^{-1}) for 300 s, and then washed for 300s.

4.7. Kinome selectivity profiling

The kinase selectivity of LC-SF-14 on the 80 kinases panel was evaluated using HTRF or ADP-Glo assays conducted by ICE Bioscience Inc., Beijing. In both assays, 100 × of the compound to be tested was transferred to a 384-well plate using ECHO, followed by the addition of 2 × kinase and metal solution, centrifugation at 1000 rpm for 1 min, and incubation at 25 °C for 10 min 2 × substrate and ATP solution prepared in kinase buffer was added to a 384-well plate, followed by centrifugation at 1000 rpm for 1 min and incubation at 25 °C for 60 min. For the HTRF assay, the kinase detection reagent contained XL665 and an antibody. The fluorescence signals at 620 nm (cryptate) and 665 nm (XL665) were recorded using a microplate reader. In the ADP-Glo assay, luminescence signals of the ADP-Glo reagent were recorded using a microplate reader. The readout value of the reaction control (1 % DMSO) was set at 0 % inhibition, and the readout value of background

(10 μM positive control) was set at 100 % inhibition; then the percent inhibition of each test solution was calculated.

% Inhibition was calculated as follows:

$$\%\ Inhibition = \left\{1 - \frac{Data_{compound} - Data_{positive}}{Data_{vehicle} - Data_{positive}}\right\} \times 100$$

$Data_{compound}$: The average ratio for the positive controls (10 μM)
$Data_{vehicle}$: The average ratio for the vehicle controls (1 % DMSO)

4.8. Cell viability assay

Cell viability was evaluated using a Cell Counting Kit-8 (CCK-8) kit (Cat. K1018; APExBIO). Cells were seeded on 96-well plates (6.0×10^3 cells/well). Once they reached 70–80 % confluence, the cells were treated with DMSO or the indicated drugs. After 24 h, cells were added to CCK-8 solution and incubated for 1 h. The absorbance was measured at 450 nm using a SpectraMax iD5 microplate reader.

4.9. Immunofluorescence

KATO III cells treated with 100 nM BGJ398 or LC-SF-14 were fixed with 2 % formaldehyde in PBS for 2 min and blocked with 5 % w/v BSA in PBS for 1 h. Cells were incubated with anti-p-ERK antibody (Cat. #R1310-10, Huabio) overnight. The cells were washed thrice with PBS and incubated with an Alexa Fluor 488-conjugated secondary antibody (Cat. #A0423; Beyotime Biotechnology) for 1 h, and stained with DAPI (4′,6diamidino-2-phenylindole, Cat. #C1002, Beyotime Biotechnology) for 10 min. Cells were observed by fluorescence microscopy using an EVOS M7000 imaging system (Thermo Fisher).

4.10. Animals

For profiling pharmacokinetic properties, LC-SF-14 was mixed in a solvent composed of 10 % N-methylpyrrolidone, 70 % saline, and 20 % PEG-400, and the pH was adjusted to 7. Male Sprague-Dawley rats were subjected to two different routes of administration of the LC-SF-14 solution. Intravenous injection was administered at a dose of 2 mg/kg, whereas oral administration was administered at a dose of 20 mg/kg. Following treatment, blood samples were drawn from each rat at 1, 2, 3, 4, 6, 8, 12, and 24 h (p.o.), or at 0.25, 0.5, 1, 2, 3, 4, 6, 8, 12, and 24 h (i.v.). The samples were centrifuged, and the plasma supernatant was obtained and subjected to LC−MS/MS analysis (Triple Quad 6500+; SCIEX).

For the xenograft model, male BALB/c nude mice (20−22 g) were divided into six distinct groups: vehicle, 10 mg/kg LC-SF-14, and 20 mg/kg LC-SF-14. Subsequently, a suspension of 5×10^6/mL SNU-16 cells was subcutaneously injected into the right flank of nude mice, eventually culminating in an average tumor volume of 50–100 mm^3. Each compound or vehicle was prepared as a solution containing 10 % N-methylpyrrolidone, 70 % saline, and 20 % PEG-400 for intragastric delivery. Control mice were orally administered equivalent volumes of vehicle. To monitor xenograft progression, the body weight and tumor volume of the subjects were measured daily. The tumor volume was quantified by precisely measuring the width (w) and length (l). Following the completion of the treatment course, tumor specimens were extracted after a 4 h post-treatment period for further analysis.

4.11. Statistics and reproducibility

Statistical analyses were performed using GraphPad Prism 8.0 (GraphPad Software). Data are expressed as the mean ± standard deviation (SD). Statistically significant differences between pairs of groups were determined using a one-way analysis of variance (ANOVA), whereas differences between multiple groups were assessed using Dunnett's multiple range test. Statistical significance was set at $P < 0.05$.

CRediT authorship contribution statement

Lei Zheng: Writing – original draft, Methodology, Investigation, Formal analysis. **Yuhan Wang:** Investigation, Formal analysis, Data curation. **Zheng Jiang:** Writing – review & editing, Methodology, Investigation. **Shiyan Chen:** Supervision, Data curation. **Xiansheng Cao:** Validation. **Xiaohao Huang:** Investigation. **Ruixiang Luo:** Supervision, Methodology. **Lulu Zheng:** Investigation. **Qin Li:** Investigation. **Linglan Tu:** Methodology. **Jie Li:** Methodology. **Guang Liang:** Writing – review & editing, Resources, Project administration. **Lingfeng Chen:** Writing – review & editing, Resources, Project administration.

Declaration of competing interest

The authors declare the following financial interests/personal relationships which may be considered as potential competing interests: Lingfeng Chen reports financial support was provided by National Natural Science Foundation of China.

Acknowledgments

This work was supported by the National Natural Science Foundation of China (82422068 to L.C.), Natural Science Funding of Zhejiang Province (LR24H300001 and LDG25H300001 to L.C.), Zhejiang Medical and Health Science Project (2023KY622 to L.Z.), and Huadong Medicine Joint Funds of Zhejiang Provincial Natural Science Foundation of China (LHDMY23H310004 to L.Z.).

Appendix A. Supplementary data

Supplementary data to this article can be found online at https://doi.org/10.1016/j.ejmech.2025.117745.

Abbreviations

BRAF, v-raf murine sarcoma viral oncogene homolog B1; CDK, cyclin-dependent kinase; DIPEA, N,N-Diisopropylethylamine; EGFR, epidermal growth factor receptor; FDA, food and drug administration; FGFR, fibroblast growth factor receptor; FRS, fibroblast growth factor receptor substrate; HATU, 2-(7-Azabenzotriazol-1-yl)-N,N,N′,N′-tetramethyluronium hexafluorophosphate HDAC, histone deacetylase; IC_{50}, a half-maximal inhibitory concentration; IPA, isopropanol; KRAS, kirsten rat sarcoma viral oncogene; PD-1, programmed death 1; PDB, protein data bank; PLCγ, phospholipase C-γ; PROTAC, proteolysis-targeting chimeric; PTP, protein tyrosine phosphatase, RTK, receptor tyrosine kinase; SAR, structure activity relationship; SD, stable disease; SH2, Src homology-2; SHP2, Src homology-2 domain-containing phosphatase 2; MAPK, mitogen-activated protein kinase; MEK, mitogen-activated extracellular signal-regulated kinase.

Data availability

Data will be made available on request.

References

[1] Y.X. Wei, X. Zhao, B.C. Zhang, Synergistic effect of moxibustion and rehabilitation training in functional recovery of post-stroke spastic hemiplegia, Compl. Ther. Med. 26 (2016) 55–60.
[2] S. Bunda, K. Burrell, P. Heir, L. Zeng, A. Alamsahebpour, Y. Kano, B. Raught, Z. Y. Zhang, G. Zadeh, M. Ohh, Inhibition of SHP2-mediated dephosphorylation of Ras suppresses oncogenesis, Nat. Commun. 6 (2015) 8859.
[3] A.D. Levy, X. Xiao, J.E. Shaw, S.P. Sudarsana Devi, S.M. Katrancha, A.M. Bennett, C.A. Greer, J.R. Howe, K. Machida, A.J. Koleske, Noonan syndrome-associated SHP2 dephosphorylates GluN2B to regulate NMDA receptor function, Cell Rep. 24 (2018) 1523–1535.
[4] M. Bentires-Alj, J.G. Paez, F.S. David, H. Keilhack, B. Halmos, K. Naoki, J.M. Maris, A. Richardson, A. Bardelli, D.J. Sugarbaker, W.G. Richards, J. Du, L. Girard, J. D. Minna, M.L. Loh, D.E. Fisher, V.E. Velculescu, B. Vogelstein, M. Meyerson, W.

R. Sellers, B.G. Neel, Activating mutations of the noonan syndrome-associated SHP2/PTPN11 gene in human solid tumors and adult acute myelogenous leukemia, Cancer Res. 64 (2004) 8816–8820.
[5] X. Yuan, H. Bu, J. Zhou, C.Y. Yang, H. Zhang, Recent advances of SHP2 inhibitors in cancer therapy: current development and clinical application, J. Med. Chem. 63 (2020) 11368–11396.
[6] Z. Song, M. Wang, Y. Ge, X.P. Chen, Z. Xu, Y. Sun, X.F. Xiong, Tyrosine phosphatase SHP2 inhibitors in tumor-targeted therapies, Acta Pharm. Sin. B 11 (2021) 13–29.
[7] Y.N. Chen, M.J. LaMarche, H.M. Chan, P. Fekkes, J. Garcia-Fortanet, M.G. Acker, B. Antonakos, C.H. Chen, Z. Chen, V.G. Cooke, J.R. Dobson, Z. Deng, F. Fei, B. Firestone, M. Fodor, C. Fridrich, H. Gao, D. Grunenfelder, H.X. Hao, J. Jacob, S. Ho, K. Hsiao, Z.B. Kang, R. Karki, M. Kato, J. Larrow, L.R. La Bonte, F. Lenoir, G. Liu, S. Liu, D. Majumdar, M.J. Meyer, M. Palermo, L. Perez, M. Pu, E. Price, C. Quinn, S. Shakya, M.D. Shultz, J. Slisz, K. Venkatesan, P. Wang, M. Warmuth, S. Williams, G. Yang, J. Yuan, J.H. Zhang, P. Zhu, T. Ramsey, N.J. Keen, W. R. Sellers, T. Stams, P.D. Fortin, Allosteric inhibition of SHP2 phosphatase inhibits cancers driven by receptor tyrosine kinases, Nature 535 (2016) 148–152.
[8] P. Hof, S. Pluskey, S. Dhe-Paganon, M.J. Eck, S.E. Shoelson, Crystal structure of the tyrosine phosphatase SHP-2, Cell 92 (1998) 441–450.
[9] Y. Song, S. Wang, M. Zhao, X. Yang, B. Yu, Strategies targeting protein tyrosine phosphatase SHP2 for cancer therapy, J. Med. Chem. 65 (2022) 3066–3079.
[10] J. Garcia Fortanet, C.H. Chen, Y.N. Chen, Z. Chen, Z. Deng, B. Firestone, P. Fekkes, M. Fodor, P.D. Fortin, C. Fridrich, D. Grunenfelder, S. Ho, Z.B. Kang, R. Karki, M. Kato, N. Keen, L.R. LaBonte, J. Larrow, F. Lenoir, G. Liu, S. Liu, F. Lombardo, D. Majumdar, M.J. Meyer, M. Palermo, L. Perez, M. Pu, T. Ramsey, W.R. Sellers, M. D. Shultz, T. Stams, C. Towler, P. Wang, S.L. Williams, J.H. Zhang, M.J. LaMarche, Allosteric inhibition of SHP2: identification of a potent, selective, and orally efficacious phosphatase inhibitor, J. Med. Chem. 59 (2016) 7773–7782.
[11] J. Wu, W. Li, Z. Zheng, X. Lu, H. Zhang, Y. Ma, R. Wang, Design, synthesis, biological evaluation, common feature pharmacophore model and molecular dynamics simulation studies of ethyl 4-(phenoxymethyl)-2-phenylthiazole-5-carboxylate as Src homology-2 domain containing protein tyrosine phosphatase-2 (SHP2) inhibitors, J. Biomol. Struct. Dyn. 39 (2021) 1174–1188.
[12] M.J. LaMarche, M. Acker, A. Argintaru, D. Bauer, J. Boisclair, H. Chan, C.H. Chen, Y.N. Chen, Z. Chen, Z. Deng, M. Dore, D. Dunstan, J. Fan, P. Fekkes, B. Firestone, M. Fodor, J. Garcia-Fortanet, P.D. Fortin, C. Fridrich, J. Giraldes, M. Glick, D. Grunenfelder, H.X. Hao, M. Hentemann, S. Ho, A. Jouk, Z.B. Kang, R. Karki, M. Kato, N. Keen, R. Koenig, L.R. LaBonte, J. Larrow, G. Liu, S. Liu, D. Majumdar, S. Mathieu, M.J. Meyer, M. Mohseni, R. Ntaganda, M. Palermo, L. Perez, M. Pu, T. Ramsey, J. Reilly, P. Sarver, W.R. Sellers, M. Sendzik, M.D. Shultz, J. Slisz, K. Slocum, T. Smith, S. Spence, T. Stams, C. Straub, V. Tamez Jr., B.B. Toure, C. Towler, P. Wang, H. Wang, S.L. Williams, F. Yang, B. Yu, J.H. Zhang, S. Zhu, Identification of TNO155, an allosteric SHP2 inhibitor for the treatment of cancer, J. Med. Chem. 63 (2020) 13578–13594.
[13] R. He, Z.H. Yu, R.Y. Zhang, L. Wu, A.M. Gunawan, B.S. Lane, J.S. Shim, L.F. Zeng, Y. He, L. Chen, C.D. Wells, J.O. Liu, Z.Y. Zhang, Exploring the existing drug space for novel pTyr mimetic and SHP2 inhibitors, ACS Med. Chem. Lett. 6 (2015) 782–786.
[14] Y.N. Chen, M.J. LaMarche, H.M. Chan, P. Fekkes, J. Garcia-Fortanet, M.G. Acker, B. Antonakos, C.H. Chen, Z. Chen, V.G. Cooke, J.R. Dobson, Z. Deng, F. Fei, B. Firestone, M. Fodor, C. Fridrich, H. Gao, D. Grunenfelder, H.X. Hao, J. Jacob, S. Ho, K. Hsiao, Z.B. Kang, R. Karki, M. Kato, J. Larrow, L.R. La Bonte, F. Lenoir, G. Liu, S. Liu, D. Majumdar, M.J. Meyer, M. Palermo, L. Perez, M. Pu, E. Price, C. Quinn, S. Shakya, M.D. Shultz, J. Slisz, K. Venkatesan, P. Wang, M. Warmuth, S. Williams, G. Yang, J. Yuan, J.H. Zhang, P. Zhu, T. Ramsey, N.J. Keen, W. R. Sellers, T. Stams, P.D. Fortin, Allosteric inhibition of SHP2 phosphatase inhibits cancers driven by receptor tyrosine kinases, Nature 535 (2016) 148–152.
[15] R.J. Nichols, F. Haderk, C. Stahlhut, C.J. Schulze, G. Hemmati, D. Wildes, C. Tzitzilonis, K. Mordec, A. Marquez, J. Romero, T. Hsieh, A. Zaman, V. Olivas, C. McCoach, C.M. Blakely, Z. Wang, G. Kiss, E.S. Koltun, A.L. Gill, M. Singh, M. A. Goldsmith, J.A.M. Smith, T.G. Bivona, RAS nucleotide cycling underlies the SHP2 phosphatase dependence of mutant BRAF-, NF1- and RAS-driven cancers, Nat. Cell Biol. 20 (2018) 1064–1073.
[16] C. Ma, D. Kang, P. Gao, W. Zhang, X. Wu, Z. Xu, H. Han, L. Zhang, Y. Cai, Y. Wang, Y. Wang, W. Long, Discovery of JAB-3312, a potent SHP2 allosteric inhibitor for cancer treatment, J. Med. Chem. 67 (2024) 13534–13549.
[17] D. Shen, W. Chen, J. Zhu, G. Wu, R. Shen, M. Xi, H. Sun, Therapeutic potential of targeting SHP2 in human developmental disorders and cancers, Eur. J. Med. Chem. 190 (2020) 112117.
[18] I. Brana, G. Shapiro, M.L. Johnson, H.A. Yu, D. Robbrecht, D.S.-W. Tan, L.L. Siu, H. Minami, N. Steeghs, T. Hengelage, E. Tan, K. Biette, K. Xu, S.E. Moody, M. Jove, Initial results from a dose finding study of TNO155, a SHP2 inhibitor, in adults with advanced solid tumors, J. Clin. Oncol. 39 (2021), 3005–3005.
[19] Z. Guo, Y. Duan, K. Sun, T. Zheng, J. Liu, S. Xu, J. Xu, Advances in SHP2 tunnel allosteric inhibitors and bifunctional molecules, Eur. J. Med. Chem. 275 (2024) 116579.
[20] L. Dardaei, H.Q. Wang, M. Singh, P. Fordjour, K.X. Shaw, S. Yoda, G. Kerr, K. Yu, J. Liang, Y. Cao, Y. Chen, M.S. Lawrence, A. Langenbucher, J.F. Gainor, L. Friboulet, I. Dagogo-Jack, D.T. Myers, E. Labrot, D. Ruddy, M. Parks, D. Lee, R. H. DiCecca, S. Moody, H. Hao, M. Mohseni, M. LaMarche, J. Williams, K. Hoffmaster, G. Caponigro, A.T. Shaw, A.N. Hata, C.H. Benes, F. Li, J. A. Engelman, SHP2 inhibition restores sensitivity in ALK-rearranged non-small-cell lung cancer resistant to ALK inhibitors, Nat. Med. 24 (2018) 512–517.
[21] C. Liu, H. Lu, H. Wang, A. Loo, X. Zhang, G. Yang, C. Kowal, S. Delach, Y. Wang, S. Goldoni, W.D. Hastings, K. Wong, H. Gao, M.J. Meyer, S.E. Moody, M. J. LaMarche, J.A. Engelman, J.A. Williams, P.S. Hammerman, T.J. Abrams, M. Mohseni, G. Caponigro, H.X. Hao, Combinations with allosteric SHP2 inhibitor TNO155 to block receptor tyrosine kinase signaling, Clin. Cancer Res. 27 (2021) 342–354.
[22] A. Drilon, M.R. Sharma, M.L. Johnson, T.A. Yap, S. Gadgeel, D. Nepert, G. Feng, M. B. Reddy, A.S. Harney, M. Elsayed, A.W. Cook, C.E. Wong, R.J. Hinklin, Y. Jiang, E. N. Brown, N.A. Neitzel, E.R. Laird, W.-I. Wu, A. Singh, P. Wei, K.A. Ching, J. J. Gaudino, P.A. Lee, D.P. Hartley, S.M. Rothenberg, SHP2 inhibition sensitizes diverse oncogene-addicted solid tumors to Re-treatment with targeted therapy, Cancer Discov. 13 (2023) 1789–1801.
[23] A. Beenken, M. Mohammadi, The FGF family: biology, pathophysiology and therapy, Nat. Rev. Drug Discov. 8 (2009) 235–253.
[24] M. Katoh, H. Nakagama, FGF receptors: cancer biology and therapeutics, Med. Res. Rev. 34 (2014) 280–300.
[25] I.S. Babina, N.C. Turner, Advances and challenges in targeting FGFR signalling in cancer, Nat. Rev. Cancer 17 (2017) 318–332.
[26] M. Katoh, Therapeutics targeting FGF signaling network in human diseases, Trends Pharmacol. Sci. 37 (2016) 1081–1096.
[27] L. Chen, Y. Zhang, L. Yin, B. Cai, P. Huang, X. Li, G. Liang, Fibroblast growth factor receptor fusions in cancer: opportunities and challenges, J. Exp. Clin. Cancer Res. 40 (2021) 345.
[28] T. Jogo, Y. Nakamura, K. Shitara, H. Bando, H. Yasui, T. Esaki, T. Terazawa, T. Satoh, E. Shinozaki, T. Nishina, Y. Sunakawa, Y. Komatsu, H. Hara, E. Oki, N. Matsuhashi, T. Ohta, T. Kato, K. Ohtsubo, T. Kawakami, N. Okano, Y. Yamamoto, T. Yamada, A. Tsuji, J.I. Odegaard, H. Taniguchi, T. Doi, S. Fujii, T. Yoshino, Circulating tumor DNA analysis detects FGFR2 amplification and concurrent genomic alterations associated with FGFR inhibitor efficacy in advanced gastric cancer, Clin. Cancer Res. 27 (2021) 5619–5627.
[29] G. Betts, H. Valentine, S. Pritchard, R. Swindell, V. Williams, S. Morgan, E. A. Griffiths, I. Welch, C. West, C. Womack, FGFR2, HER2 and cMet in gastric adenocarcinoma: detection, prognostic significance and assessment of downstream pathway activation, Virchows Arch. 464 (2014) 145–156.
[30] M.H. Schafer, P. Lingohr, A. Strasser, N.C. Lehnen, M. Braun, S. Perner, T. Holler, G. Kristiansen, J.C. Kalff, I. Gutgemann, Fibroblast growth factor receptor 1 gene amplification in gastric adenocarcinoma, Hum. Pathol. 46 (2015) 1488–1495.
[31] G. Piro, C. Carbone, I. Cataldo, F. Di Nicolantonio, S. Giacopuzzi, G. Aprile, F. Simionato, F. Boschi, M. Zanotto, M.M. Mina, R. Santoro, V. Merz, A. Sbarbati, G. de Manzoni, A. Scarpa, G. Tortora, D. Melisi, An FGFR3 autocrine loop sustains acquired resistance to trastuzumab in gastric cancer patients, Clin. Cancer Res. 22 (2016) 6164–6175.
[32] Y. Loriot, A. Necchi, S.H. Park, J. Garcia-Donas, R. Huddart, E. Burgess, M. Fleming, A. Rezazadeh, B. Mellado, S. Varlamov, M. Joshi, I. Duran, S. T. Tagawa, Y. Zakharia, B. Zhong, K. Stuyckens, A. Santiago-Walker, P. De Porre, A. O'Hagan, A. Avadhani, A.O. Siefker-Radtke, B.L.C.S. Group, Erdafitinib in locally advanced or metastatic urothelial carcinoma, N. Engl. J. Med. 381 (2019) 338–348.
[33] H. Patani, T.D. Bunney, N. Thiyagarajan, R.A. Norman, D. Ogg, J. Breed, P. Ashford, A. Potterton, M. Edwards, S.V. Williams, G.S. Thomson, C.S. Pang, M. A. Knowles, A.L. Breeze, C. Orengo, C. Phillips, M. Katan, Landscape of activating cancer mutations in FGFR kinases and their differential responses to inhibitors in clinical use, Oncotarget 7 (2016) 24252–24268.
[34] G.K. Abou-Alfa, V. Sahai, A. Hollebecque, G. Vaccaro, D. Melisi, R. Al-Rajabi, A. S. Paulson, M.J. Borad, D. Gallinson, A.G. Murphy, D.Y. Oh, E. Dotan, D. V. Catenacci, E. Van Cutsem, T. Ji, C.F. Lihou, H. Zhen, L. Feliz, A. Vogel, Pemigatinib for previously treated, locally advanced or metastatic cholangiocarcinoma: a multicentre, open-label, phase 2 study, Lancet Oncol. 21 (2020) 671–684.
[35] D. Romero, Benefit from pemigatinib in cholangiocarcinoma, Nat. Rev. Clin. Oncol. 17 (2020) 337.
[36] V. Subbiah, V. Sahai, D. Maglic, K. Bruderek, B.B. Toure, S. Zhao, R. Valverde, P. J. O'Hearn, D.T. Moustakas, H. Schonherr, N. Gerami-Moayed, A.M. Taylor, B. M. Hudson, D.J. Houde, D. Pal, L. Foster, H. Gunaydin, P. Ayaz, D.A. Sharon, L. Goyal, A.M. Schram, S. Kamath, C.A. Sherwin, O. Schmidt-Kittler, K.Y. Jen, F. Ricard, B.B. Wolf, D.E. Shaw, D.A. Bergstrom, J. Watters, J.B. Casaletto, RLY-4008, the first highly selective FGFR2 inhibitor with activity across FGFR2 alterations and resistance mutations, Cancer Discov. 13 (2023) 2012–2031.
[37] I.M. Silverman, A. Hollebecque, L. Friboulet, S. Owens, R.C. Newton, H. Zhen, L. Feliz, C. Zecchetto, D. Melisi, T.C. Burn, Clinicogenomic analysis of FGFR2-Rearranged cholangiocarcinoma identifies correlates of response and mechanisms of resistance to pemigatinib, Cancer Discov. 11 (2021) 326–339.
[38] Y. Chong, Y. Liu, S. Lu, B. Cai, H. Qin, C.S. Chang, M. Ren, J.K. Cowell, T. Hu, Critical individual roles of the BCR and FGFR1 kinase domains in BCR-FGFR1-driven stem cell leukemia/lymphoma syndrome, Int. J. Cancer 146 (2020) 2243–2254.
[39] H. Lu, C. Liu, R. Velazquez, H. Wang, L.M. Dunkl, M. Kazic-Legueux, A. Haberkorn, E. Billy, E. Manchado, S.M. Brachmann, S.E. Moody, J.A. Engelman, P. S. Hammerman, G. Caponigro, M. Mohseni, H.X. Hao, SHP2 inhibition overcomes RTK-mediated pathway reactivation in KRAS-mutant tumors treated with MEK inhibitors, Mol. Cancer Therapeut. 18 (2019) 1323–1334.
[40] A. Anighoro, J. Bajorath, G. Rastelli, Polypharmacology: challenges and opportunities in drug discovery, J. Med. Chem. 57 (2014) 7874–7887.
[41] E. Proschak, H. Stark, D. Merk, Polypharmacology by design: a medicinal chemist's perspective on multitargeting compounds, J. Med. Chem. 62 (2019) 420–444.
[42] J. Lötsch, G. Geisslinger, Low-dose drug combinations along molecular pathways could maximize therapeutic effectiveness while minimizing collateral adverse effects, Drug Discov. Today 16 (2011) 1001–1006.

[43] M. Liu, S. Gao, T. Liang, X. Qiu, X. Yang, H. Fang, X. Hou, Discovery of novel src Homology-2 domain-containing phosphatase 2 and histone deacetylase dual inhibitors with potent antitumor efficacy and enhanced antitumor immunity, J. Med. Chem. 65 (2022) 12200–12218.
[44] X. Chen, C. Shu, W. Li, Q. Hou, G. Luo, K. Yang, X. Wu, Discovery of a novel src Homology-2 domain containing protein tyrosine Phosphatase-2 (SHP2) and cyclin-dependent kinase 4 (CDK4) dual inhibitor for the treatment of triple-negative breast cancer, J. Med. Chem. 65 (2022) 6729–6747.
[45] M. Wang, J. Lu, M. Wang, C.Y. Yang, S. Wang, Discovery of SHP2-D26 as a first, potent, and effective PROTAC degrader of SHP2 protein, J. Med. Chem. 63 (2020) 7510–7528.
[46] L. Ma, Y. Li, R. Luo, Y. Wang, J. Cao, W. Fu, B. Qian, L. Zheng, L. Tang, X. Lv, L. Zheng, G. Liang, L. Chen, Discovery of a selective and orally bioavailable FGFR2 degrader for treating gastric cancer, J. Med. Chem. 66 (2023) 7438–7453.
[47] R. Luo, W. Fu, J. Shao, L. Ma, S. Shuai, Y. Xu, Z. Jiang, Z. Ye, L. Zheng, L. Zheng, J. Yu, Y. Zhang, L. Yin, L. Tu, X. Lv, J. Li, G. Liang, L. Chen, Discovery of a potent and selective allosteric inhibitor targeting the SHP2 tunnel site for RTK-Driven cancer treatment, Eur. J. Med. Chem. 253 (2023) 115305.
[48] J. Gattineni, P. Alphonse, Q. Zhang, N. Mathews, C.M. Bates, M. Baum, Regulation of renal phosphate transport by FGF23 is mediated by FGFR1 and FGFR4, Am. J. Physiol-renal. 306 (2014) F351–F358.
[49] F. Sacco, L. Perfetto, L. Castagnoli, G. Cesareni, The human phosphatase interactome: an intricate family portrait, FEBS Lett. 586 (2012) 2732–2739.
[50] L. Hu, M. Fan, S. Shi, X. Song, F. Wang, H. He, B. Qi, Dual target inhibitors based on EGFR: promising anticancer agents for the treatment of cancers (2017-), Eur. J. Med. Chem. 227 (2022) 113963.